A germline point mutation in the MYC-FBW7 phosphodegron initiates hematopoietic malignancies

Brian Freie,[1] Patrick A. Carroll,[1] Barbara J. Varnum-Finney,[2] Erin L. Ramsey,[1] Vijay Ramani,[3] Irwin Bernstein,[2] and Robert N. Eisenman[1]

[1]Basic Sciences Division, Fred Hutchinson Cancer Center, Seattle, Washington 98109, USA; [2]Clinical Research Division, Fred Hutchinson Cancer Center, Seattle, Washington 98109, USA; [3]Gladstone Institute for Data Science and Biotechnology, University of California, San Francisco, San Francisco, California 94158, USA

Oncogenic activation of MYC in cancers predominantly involves increased transcription rather than coding region mutations. However, MYC-dependent lymphomas frequently acquire point mutations in the MYC phosphodegron, including at threonine 58 (T58), where phosphorylation permits binding via the FBW7 ubiquitin ligase triggering MYC degradation. To understand how T58 phosphorylation functions in normal cell physiology, we introduced an alanine mutation at T58 (T58A) into the endogenous *c-Myc* locus in the mouse germline. While MYC-T58A mice develop normally, lymphomas and myeloid leukemias emerge in ~60% of adult homozygous T58A mice. We found that primitive hematopoietic progenitor cells from MYC-T58A mice exhibit aberrant self-renewal normally associated with hematopoietic stem cells (HSCs) and up-regulate a subset of MYC target genes important in maintaining stem/progenitor cell balance. In lymphocytes, genomic occupancy by MYC-T58A was increased at all promoters compared with WT MYC, while genes differentially expressed in a T58A-dependent manner were significantly more proximal to MYC-bound enhancers. MYC-T58A lymphocyte progenitors exhibited metabolic alterations and decreased activation of inflammatory and apoptotic pathways. Our data demonstrate that a single point mutation stabilizing MYC is sufficient to skew target gene expression, producing a profound gain of function in multipotential hematopoietic progenitors associated with self-renewal and initiation of lymphomas and leukemias.

[*Keywords*: FBW7; leukemia; MYC; hematopoiesis; lymphoma; progenitor cells; protein stability; self-renewal]

Supplemental material is available for this article.

Received October 23, 2023; revised version accepted March 19, 2024.

The *MYC* gene family is essential for normal development and cell physiology and is deregulated in an extraordinarily wide range of cancers. The c-*MYC* gene (referred to here as *MYC*) is induced in response to numerous cytokines, growth factors, or other mitogenic signals. Serum- and ligand-stimulated pathways (such as Notch, Sonic Hedgehog, Wnt, EGF, PDGF, and others) activate *MYC* gene expression as an early and robust target. However, depending on context, this response can be limited by the tight regulation of MYC at multiple levels (e.g., transcription initiation and pausing, RNA stability and export, translation, and protein half-life) (for recent review, see Dhanasekaran et al. 2022).

In a large subset of cancers, the tight regulation of MYC is lost; *MYC* RNA is increased and is not down-regulated in response to differentiation signals or mitogen removal, resulting in increased protein abundance. This deregulation of *MYC* expression can be due to rearrangements involving *MYC* genomic loci, including chromosomal translocations, gene amplification, viral insertions and transductions, or gain-of-function mutations in one or more signal transduction pathways known to induce *Myc* expression (Dalla-Favera et al. 1982; Nowell et al. 1983; Adams et al. 1985; He et al. 1998). In each case, *MYC* expression is uncoupled from its normal physiological regulators. Indeed, even relatively low levels of deregulated *MYC* expression can cause profound changes in cell biology (Smith et al. 2006; Murphy et al. 2008).

MYC activity is also regulated by modification of MYC protein. Perhaps the most crucial region of the MYC protein required for this post-translational regulation is located in the transactivation domain in a conserved region known as MYC box I (for review, see Farrell and Sears

Corresponding authors: eisenman@fredhutch.org, bfreie@fredhutch.org
Article published online ahead of print. Article and publication date are online at http://www.genesdev.org/cgi/doi/10.1101/gad.351292.123. Freely available online through the *Genes & Development* Open Access option.

2014). The established function of this region is as a phosphodegron in which phosphorylation of MYC contributes to the regulation of MYC protein stability (Pulverer et al. 1994). Within murine MYC box 1, the amino acid sequence from residues 57–63 (PTPPLSP; corresponding to residues 72–78 in human MYC) is of critical importance (Flinn et al. 1998; Salghetti et al. 1999). The growth-regulated kinase GSK3β phosphorylates threonine at amino acid 58 (T58), resulting in binding by the F-box protein Fbw7 (a subunit of the SCF ubiquitin ligase complex), which ubiquitinates MYC, targeting it for proteasome-mediated degradation (Pulverer et al. 1994; Gregory et al. 2003; Welcker et al. 2004; Yada et al. 2004). A recent study showed that MYC-FBW7 interaction involves an FBW7 dimer and is also stabilized by phosphorylation at MYC-T244 (Welcker et al. 2022). MYC protein containing nonphosphorylated T58 is not efficiently bound by Fbw7 and exhibits increased stability. Mitogen-induced cell proliferation also triggers phosphorylation of S62 within MYC box 1 through RAS–ERK signaling and CDKs. Phosphorylation of S62 primes GSK3β binding to, and subsequent phosphorylation of, T58 (Sears et al. 2000). Thus, MYC degradation is controlled through multiple kinases and is closely tied to signal transduction pathways.

Early studies found that point mutations of T58 (or its adjacent amino acid residues in MYC box I) that disrupt T58 phosphorylation were frequently observed in translocated *MYC* alleles in Burkitt's lymphoma, AIDS-related lymphomas, and B-cell acute lymphoblastic lymphoma (Bhatia et al. 1993, 1994). Furthermore, three of the four transforming retroviruses from which the v-myc oncogene was originally identified also contain mutations in the cognate MYC box I threonine (Bhatia et al. 1993). Therefore, mutations that disrupt T58 phosphorylation are selected genetic events acquired during initiation or progression of MYC-associated cancers. When MYC mutated at threonine 58 to alanine (T58A) was ectopically overexpressed by retrovirus in mouse hematopoietic cells, B-cell lymphomas evolved faster than those generated by overexpressing normal, wild-type MYC (Hemann et al. 2005). In other studies, MYC-T58A overexpressed in mouse mammary tissue induced mammary carcinomas more rapidly than wild-type c-MYC (Wang et al. 2011). These studies indicated that MYC blocked for phosphorylation at T58 is associated with increased oncogenicity compared with wild-type MYC. Indeed, T58 mutated MYC has been widely used in experimental models to increase and accelerate tumorigenesis (Swartling et al. 2012; Chalishazar et al. 2019). Moreover, ectopic expression of MYC-T58A maintained pluripotency in murine embryonic stem (ES) cells independent of leukemia inhibitory factor (LIF) (Cartwright et al. 2005).

Interestingly, only a partial increase in MYC protein stability is seen when T58 is mutated, consistent with the fact that MYC stability is controlled by other pathways independent of T58 phosphorylation (Kim et al. 2003; Welcker et al. 2004; Schukur et al. 2020). Furthermore, evidence suggests that the T58 mutation is frequently acquired in tumors that already contain deregulated and highly expressed MYC (Bhatia et al. 1994). In addition, while it has been well established that deregulated MYC triggers apoptosis, the T58A mutant MYC actually results in decreased apoptosis when overexpressed (Hemann et al. 2005). Taken together, these findings suggest that T58 phosphorylation may affect MYC activity by coupling degradation with MYC function in an as yet undefined way.

The previous studies on T58A and other MYC mutations were carried out using exogenous, overexpressed, and deregulated MYC. To separate the effects of T58 mutation from the profound effects observed when MYC is overexpressed, we sought to study MYC regulation by T58 phosphorylation in a setting in which MYC expression is not overtly deregulated. To do this, we introduced a point mutation in murine MYC by changing T58 to alanine (T58A) in the endogenous *Myc* locus in the mouse germline. In this way, we generated mice that express MYC protein mutated at T58 but retain the normal genomic regulation of MYC. Here we report that this mutation causes a tumor-prone phenotype associated with aberrant hematopoietic progenitor cell self-renewal and altered transcriptional regulation of loci proximal to MYC-bound enhancers.

Results

Generation of mice with a threonine-58-to-alanine mutation in endogenous Myc

We generated mice with a targeted mutation of threonine 58 to alanine (T58A) in the endogenous c-*myc* allele (referred to here as *Myc*) in mice using standard transgenic techniques. The endogenous *Myc* locus was targeted in ES cells using a construct containing the T58A mutation in exon 2 of *Myc* (Supplemental Fig. S1A). Chimeric mice were generated that transmitted the allele to the germline, and subsequent breeding of founders resulted in a mouse line referred to here as *Myc-T58A*. Mice heterozygous for the T58A mutation were used to breed homozygous ($Myc^{T58A/T58A}$, referred to here as *Myc-T58A*), heterozygous ($Myc^{+/T58A}$), and wild-type ($Myc^{+/+}$) littermate mice that were used for further experiments. We observed approximately normal Mendelian frequencies (Supplemental Fig. S1B) and no evidence of developmental abnormalities in either $Myc^{+/T58A}$ or $Myc^{T58A/T58A}$ mice, indicating that mice do not require phosphorylation of MYC at threonine 58 for development.

Myc-T58A *mouse tissues do not exhibit increased cell cycling or hyperplasia*

In the context of ectopic MYC expression, mutation of T58 has been demonstrated to interfere with Fbw7-mediated degradation and augment MYC protein half-life (Welcker et al. 2004; Yada et al. 2004). We measured MYC protein levels by Western blot in the spleen and thymus to determine the extent to which T58A mutation in the endogenous *Myc* gene alters steady-state MYC levels. The level of MYC protein in the $Myc^{T58A/T58A}$ knock-in mice was generally elevated approximately twofold in hematopoietic tissues such as the spleen and thymus (Fig. 1A,B; Supplemental Fig. S1C). This correlated with a half-life of T58A mutant

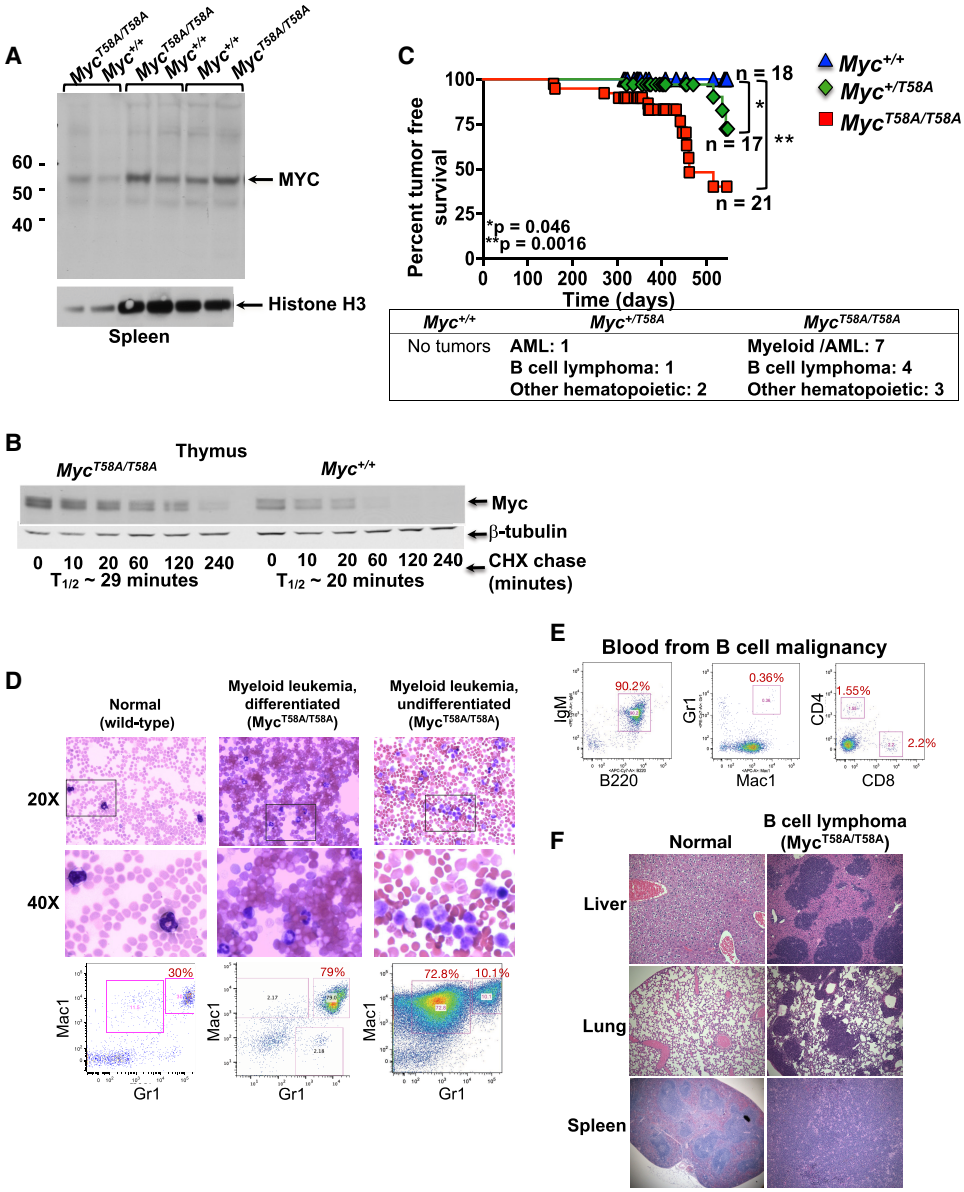

Figure 1. *Myc*$^{T58A/T58A}$ mutant mice exhibit increased MYC stability and are sensitized to late-onset hematopoietic malignancies. (*A*) Protein isolated from whole-cell extracts of spleens or thymuses from *Myc*$^{T58A/T58A}$ and littermate control mice were analyzed by Western blotting. Littermate pairs were loaded into adjacent lanes (indicated by brackets) by an investigator blind to the genotypes and blotted, and blots were detected using antibody to Myc, with Histone H3 used as a loading control. (*B*) Single-cell suspensions from *Myc*$^{T58A/T58A}$ and littermate control (*Myc*$^{+/+}$) mouse thymuses were suspended in culture media in the presence of cycloheximide for the time indicated, and Western blots for Myc and β-tubulin (loading control) were performed. One of three independent experiments with similar results is shown. The calculated half-life ($T_{1/2}$) (see Supplemental Fig. S1D) from the three experiments is indicated. (*C*) Twenty-one *Myc*$^{T58A/T58A}$, 17 *Myc*$^{T58A/+}$, and 18 littermate control *Myc*$^{+/+}$ mice were allowed to age until the development of disease. Mice were necropsied, and malignancies were confirmed using flow cytometry and pathological analysis. The data shown are a Kaplan–Meier plot of tumor-free survival. The asterisk denotes significant *P*-values for Myc$^{T58A/T58A}$ and Myc$^{+/T58A}$ mice compared with *Myc*$^{+/+}$ mice. Seven of 21 *Myc*$^{T58A/T58A}$ mice developed myeloid leukemias, and four of 21 mice developed B-cell lymphomas (with three of uncertain lineage). One of 17 *Myc*$^{+/T58A}$ mice developed myeloid leukemias, and one developed B-cell lymphomas (with two of uncertain lineage). A summary of observed malignancies is shown in the table (see also Supplemental Fig. S1I,J). (*D–F*) Mice that exhibited a detectable tumor mass or were moribund were sacrificed. (*D*) Tissues and blood smears were prepared from one normal mouse and two malignant mice (one relatively undifferentiated) and stained (Romanowsky stain). Magnifications of 20× and 40× (boxed region from 20×) are shown. Single-cell suspensions from malignant *Myc*$^{T58A/T58A}$ or control *Myc*$^{+/+}$ mice were prepared from blood, bone marrow, and spleens and analyzed by flow cytometry using antibodies specific for the indicated cell surface markers (Mac1 and Gr1) to identify differentiated myeloid cells. Cell populations were gated on live cells (DAPI-negative). Flow data are shown for *Myc*$^{+/+}$ and relatively differentiated and undifferentiated myeloid leukemias from *Myc*$^{T58A/T58A}$ mice. Flow cytometry for myeloid markers is shown. (*E*) Representative flow cytometry for a B-cell lymphoma from a malignant *Myc*$^{T58A/T58A}$ mouse. (*F*) Tissues from the malignant animal shown in *E* (liver, lung, and spleen) were stained (hematoxylin and eosin) for microscopic analysis.

MYC protein over wild-type MYC from ~20 to 30 min (Fig. 1B; Supplemental Fig. S1D). Increased *Myc* expression, resulting in higher steady-state levels of MYC protein (Fig. 1A), is typically associated with profound increases in cell proliferation. We tested whether the relatively modest increase of MYC levels in c-Myc-T58A mice might result in increased cell proliferation in different tissues. We observed no evidence of increased proliferation or hyperplasia in the lungs, brain, colon, small intestine, kidneys, or any hematopoietic organs (Supplemental Fig. S1E,F). Therefore, our MYC-T58A mouse model is distinct from previous mouse models in which increased proliferation and hyperplasia were observed when MYC was deregulated, which was associated with even relatively low levels of expression (Smith et al. 2006; Murphy et al. 2008). These data indicate that the T58A mutant *Myc* gene maintained in its normally regulated endogenous setting does not elicit the acute proliferation and hyperplasia normally associated with MYC overexpression and genomic deregulation in mice. In the following experiments, we examined the consequences of endogenously expressed wild-type and T58A MYC.

Targeting of Myc-T58A *results in sensitivity to late-onset hematopoietic malignancies*

Although we did not observe effects of the MYC-T58A mutation on development or hyperplasia, we nevertheless monitored $Myc^{+/+}$, $Myc^{+/T58A}$, and $Myc^{T58A/T58A}$ mice up to 1.5 yr of age to determine whether they would develop malignancy with a longer latency. We began to observe some hematopoietic malignancies in $Myc^{T58A/T58A}$ mice at ~6 mo of age, which ultimately affected ~60% of these mice by 1.5 yr (Fig. 1C). These malignancies were either myeloid or B lymphoid in origin (see Supplemental Fig. S1H). Myeloid malignancies presented with severe anemia and thrombocytopenia, and malignant cells were characterized by mature or immature myeloid forms expressing myeloid markers (Mac1 and Gr1) (Fig. 1D). Disruption of organ architecture was also seen in the marrow and spleen, and often in the liver and lungs (Supplemental Fig. S1G). Lymphomas were observed in peripheral blood and lymphoid organs (lymph nodes and spleen) and often disseminated into the liver and lungs (Fig. 1D). These malignant cells expressed B220 and IgM, indicating that they were mature B-cell lymphomas (Fig. 1E,F). Some myeloid and lymphoid malignancies were also seen in the $Myc^{+/T58A}$ mice, albeit to a lesser extent, indicating that a single mutant T58A *Myc* allele can sensitize mice to malignancy (see Supplemental Fig. S1H). Overall, our data indicate that these mice are predisposed to hematopoietic malignancies that require a long latency to develop. Notably, this is very different compared with a model in which MYC is overtly overexpressed, such as Eμ-MYC mice, which develop lethal tumors by ~6 mo of age (Adams et al. 1985; Eischen et al. 1999).

Hematopoietic progenitors from $Myc^{T58A/T58A}$ *mice are resistant to apoptosis*

The relatively long latency required for tumor formation indicates that malignant evolution in these mice is accompanied by the accumulation of genetic mutations over time. We therefore hypothesized that the mechanism of malignancy in T58A mutant mice is a consequence of some property in their hematopoietic cells that facilitates accumulation of additional genetic events, eventually resulting in the emergence of tumor-initiating cells. Importantly, we did not detect increased cell cycling, hyperplasia, or expansion of any particular cell population in any mature hematopoietic lineage or observe increased cellularity in the marrow, spleen, thymus, or other hematopoietic organs of young or adult *Myc-T58A* mice up to 12 wk of age (Supplemental Fig. S2A–D). Hematopoietic precursor cells in the stem or progenitor compartment are typically the cells that become transformed during malignant progression (Langdon et al. 1986; Harris et al. 1988; Krivtsov et al. 2006). Therefore, we tested whether immature hematopoietic stem or progenitor cells from $Myc^{T58A/T58A}$ mice had any measurable, intrinsic gain of function in biological activity that might be associated with leukemic stem cells prior to the onset of malignancy in young mice (8 wk old). We observed a modest reduction in the absolute number of phenotypically defined hematopoietic stem cells (HSCs; $Lin^{-}Sca1^{+}ckit^{+}CD150^{+}$), indicating a potential consequence of T58A mutation in the stem/progenitor cell compartment (Fig. 2A). We therefore assessed whether primitive, reconstituting hematopoietic stem cells (HSCs) or hematopoietic progenitors from $Myc^{T58A/T58A}$ mice exhibit increased cell cycling. We found no increase in percent S phase in $Myc^{T58A/T58A}$ mice as assessed by Ki67 staining using flow cytometry in HSCs, multipotential progenitors (MPPs), or myeloid lineage-restricted progenitors, indicating that these cells cycle at approximately the same rate (Supplemental Fig. S2E).

We next questioned whether T58 phosphorylation of endogenous *Myc* alters the balance between cell survival and apoptosis in hematopoietic precursors. We induced apoptosis in *Myc-T58A*-derived cells by culturing cells in the absence of cytokines that are required for hematopoietic cell survival. Bone marrow cells from 8-wk-old *Myc-T58A* and wild-type control mice were cultured for 24–72 h in the absence of cytokines to induce apoptosis and were subsequently replated into secondary clonogenic cultures to measure the loss of hematopoietic progenitor colony-forming unit (CFU) activity. We found that in the absence of cytokines, progenitors from $Myc^{T58A/T58A}$ mice exhibited approximately twofold increased survival compared with $Myc^{+/+}$ progenitors (Supplemental Fig. S2F). This correlated with a twofold decrease in apoptosis as measured by levels of active caspase 3 in committed myeloid progenitor cells (Supplemental Fig. S2G). We also noticed a modest but statistically significant resistance to apoptosis induced by culture in the absence of cytokine in bone marrow-derived pre-B cells from $Myc^{T58A/T58A}$ mice compared with wild-type controls (Supplemental Fig. S2H,I). Together, these data indicate that phosphorylation of MYC-T58 contributes to regulation of apoptosis in hematopoietic progenitors during normal hematopoiesis.

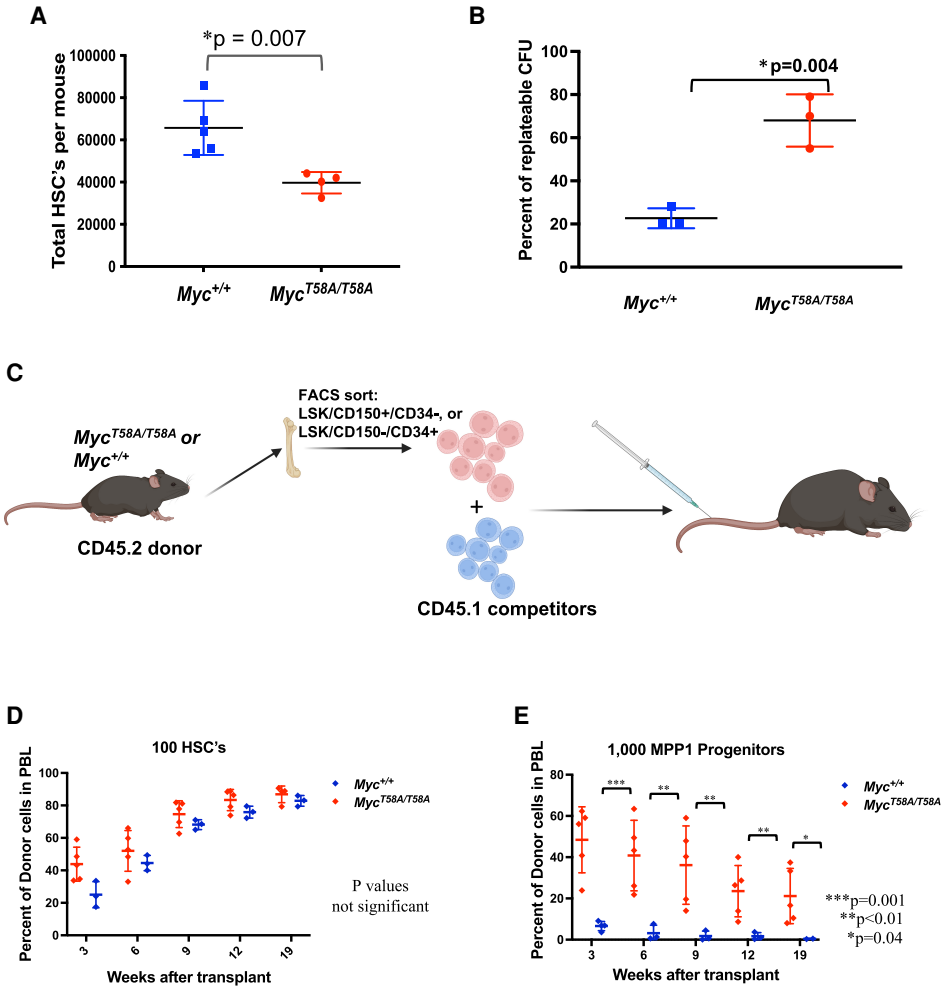

Figure 2. Aberrant self-renewal of hematopoietic progenitors from $Myc^{T58A/T58A}$ mice. (*A*) Bone marrow cells were isolated from $Myc^{T58A/T58A}$ and $Myc^{+/+}$ control littermate mice and labeled with fluorescent antibodies to enumerate hematopoietic stem cells ($Lin^{-}ckit^{+}Sca1^{+}CD150^{+}$). The data are expressed as total number of HSCs per mouse. Four mice per genotype are represented on the graph. (*B*) Bone marrow hematopoietic progenitors were cultured from either $Myc^{T58A/T58A}$ or $Myc^{+/+}$ mice in clonogenic methylcellulose assays in the presence of cytokines to support the growth of myeloid progenitor colonies. After 10 d in culture, individual colonies were picked and replated as secondary cultures supplemented with cytokines. Secondary colony formation was scored at day 10 as replatable CFU, and the ratios of replatable colonies compared with total colonies plated are shown (*y*-axis). Asterisks depict significance as assessed by *t*-test. The data shown are representative of two independent experiments. (*C–E*) Hematopoietic stem and progenitor cells from the bone marrow of three pooled $Myc^{T58A/T58A}$ mice and $Myc^{+/+}$ control littermates were sorted by flow cytometry. Hematopoietic stem cells (HSCs) and one population of multipotential progenitors (called MPP1) were sorted based on expression of the indicated cell surface markers (see Supplemental Fig. S2K). The sorted stem or progenitor cells (CD45.2) were then mixed with competitor cells (CD45.1) and transplanted into lethally irradiated recipient mice. Antibodies specific to the two CD45 isoforms were used to determine the levels of reconstitution from the indicated sorted cell populations. The data are shown as percent CD45.2 donor. Asterisks depict significance as assessed by *t*-test. The data shown are a representative of two independent experiments with similar results.

Hematopoietic progenitors in $Myc^{T58A/T58A}$ *mice exhibit aberrant self-renewal activity*

The hallmark of HSC activity is the ability to self-renew, a trait that is often acquired by leukemic cells in non-self-renewing progenitor populations (Krivtsov et al. 2006). We hypothesized that the MYC-T58A mutation potentiates self-renewal in hematopoietic progenitors that normally do not possess self-renewal activity, thus providing these cells with aberrant activity that allows them to emerge as leukemic precursors. To address this possibility, we cultured hematopoietic progenitors in vitro in clonogenic assays and assessed the ability of daughter cells from these colonies to self-renew by replating them in secondary cultures. Hematopoietic progenitors derived from $Myc^{T58A/T58A}$ mice formed colonies in secondary culture at a threefold higher frequency than progenitors from wild-type littermate control mice (Fig. 2B). These in vitro data provide evidence of an abnormal gain of function in self-renewal of $Myc^{T58A/T58A}$ hematopoietic

progenitors. To measure the self-renewal capacity of hematopoietic stem and progenitor cells more definitively in vivo, we sorted hematopoietic precursor populations from $Myc^{T58A/T58A}$ and wild-type littermate control mice (Supplemental Fig. S2J) and compared the abilities of distinct stem and progenitor cells to reconstitute lethally irradiated recipients (Fig. 2C). Sorted hematopoietic stem cells (HSCs), multipotential progenitors (MPPs), and committed myeloid progenitors (CMPs) were transplanted at dilution along with "competitor" cells (expressing distinct CD45 antigens) and analyzed over time in recipient mice for the presence of cells derived from the transplanted progenitors. HSCs are unique in their capacity to reconstitute the hematopoietic system of lethally irradiated recipient mice long-term, while multipotential progenitors and committed myeloid progenitors do not possess this ability. Strikingly, however, $Myc^{T58A/T58A}$ MPPs reconstituted lethally irradiated mice up to at least 19 wk after transplant, indicating aberrant long-term self-renewal activity (Fig. 2D,E; Supplemental Fig. S2K). Importantly we observed both myeloid and lymphoid long-term reconstitution in these mice. As expected, MPPs derived from wild-type control littermate mice exhibited no self-renewal. Taken together, the evidence indicates a striking aberrant self-renewal of MYC-T58A mutant hematopoietic progenitors that is likely to be a key factor in sensitizing these mice to myeloid neoplasia. Furthermore, both the in vitro culture and in vivo transplant data indicate that this phenotype is intrinsic to hematopoietic progenitors and not a consequence of changes in the bone marrow niche or microenvironment.

Identification and characterization of hematopoietic progenitors with increased self-renewal in MYC-T58A mutant mice

To further identify and characterize hematopoietic progenitor populations in MYC-T58A mutant mice, we used single-cell methods to profile the transcriptional outcome and epigenetic state of hematopoietic stem and progenitor cells in 8-wk-old mice prior to the onset of any disease. $Lin^{-}Sca1^{+}ckit^{+}$ cells from littermate WT and $Myc^{T58A/T58A}$ mice were obtained and sorted from bone marrow in two replicate experiments. These cells were processed using single-cell capture and barcoding for multiome RNA-seq and ATAC-seq (Supplemental Fig. S3A).

The results for captured WT and T58A single cells were pooled in the subsequent analysis, and the data sets were filtered for high-quality cells and integrated to account for technical variability (Butler et al. 2018; Hafemeister and Satija 2019; Stuart et al. 2021). Dimension reduction and clustering of these cells revealed the existence of 14 components, comprising major stem and progenitor subsets. Most of these subsets were easily identified based on the expression of defining genes for different lineages (see the Materials and Methods; Supplemental Fig. S3B). We further refined these progenitor subsets based on recently described analytical approaches and single-cell data (Cabezas-Wallscheid et al. 2014; Eaves 2015; Nestorowa et al. 2016; Belluschi et al. 2018; Rodriguez-Fraticelli et al. 2018; Konturek-Ciesla et al. 2023). There were no marked changes in the relative number or percent of any defined progenitor type upon integration of the WT and T58A data (Fig. 3A; Supplemental Fig. S3C). Lymphoid and myeloid populations ordered in pseudotime indicated that T58A progenitors did not have an obviously compromised differentiation status (Supplemental Fig. S3D).

We next asked whether the multipotential progenitor subsets in T58A mice with aberrant self-renewal (Fig. 2D) exhibit a differential gene expression signature. We compared gene expression in WT versus T58A progenitor cell populations in the integrated data. This analysis revealed that 139 genes were differentially expressed over all T58A mutant stem and progenitor cell populations (by Wilcoxon rank sum test, adjusted P value < 0.05). The fold changes in gene expression were relatively modest, and the overwhelming majority of differentially expressed genes were observed in the primitive and multipotential progenitors, with fewer changes in the most primitive HSC compartment or relatively mature progenitors (Fig. 3B,C). Differentially expressed genes were enriched for pathways that regulate hematopoiesis, particularly inflammation (such as TNF and NFκB signaling) and differentiation (Foxo1 and Spi1 target genes) (Supplemental Fig. S3E). We found increased expression of important transcription factors that mediate HSC and leukemic cell self-renewal, including nuclear hormone receptors (Nr4a1 and Nr4a2), Egr family members (Egr1 and Egr3), and chromatin modifiers (Kdm6b and Hmga2), many of which are known to be regulated by MYC (Fig. 3C,D; Supplemental Fig. S3F; Scheicher et al. 2015; Mallaney et al. 2019; Desterke et al. 2021; Sheng et al. 2021). We also noted increased expression of Pvt1, which is a long noncoding RNA often coamplified with MYC in oncogenesis and associated with increased MYC stability and expression (Tseng et al. 2014; Cho et al. 2018). Although the expression of these genes varied depending on the population, the changes were particularly evident in the most proliferative progenitor compartments (MPP_LPrimed, MPP_MPrimed, and MPP_Prolif), with a core set of 11 genes up-regulated in all three of these populations (Fig. 3C). This is consistent with the observation that Myc expression is highest in these cell populations (Supplement Fig. S3B). Overall, these data indicate that multipotential progenitors (with aberrant self-renewal capacity) in the marrow of $Myc^{T58A/T58A}$ mice have only mild, if any, disruptions in differentiation status prior to onset of detectable disease. However, they did exhibit consistent differential expression of MYC-regulated genes known to be important in differentiation, inflammation, and maintenance of the primitive hematopoietic compartment.

The chromatin accessibility of each progenitor population, as identified based on RNA-seq clustering, was assessed using the associated ATAC-seq data. To determine whether accessible regions had altered transcriptional activity, we performed DNA binding motif analysis using Chromvar to assign a motif score to every cell for all motifs in the JASPAR database (Schep et al. 2017) based on accessible peaks. Interestingly, the MYC

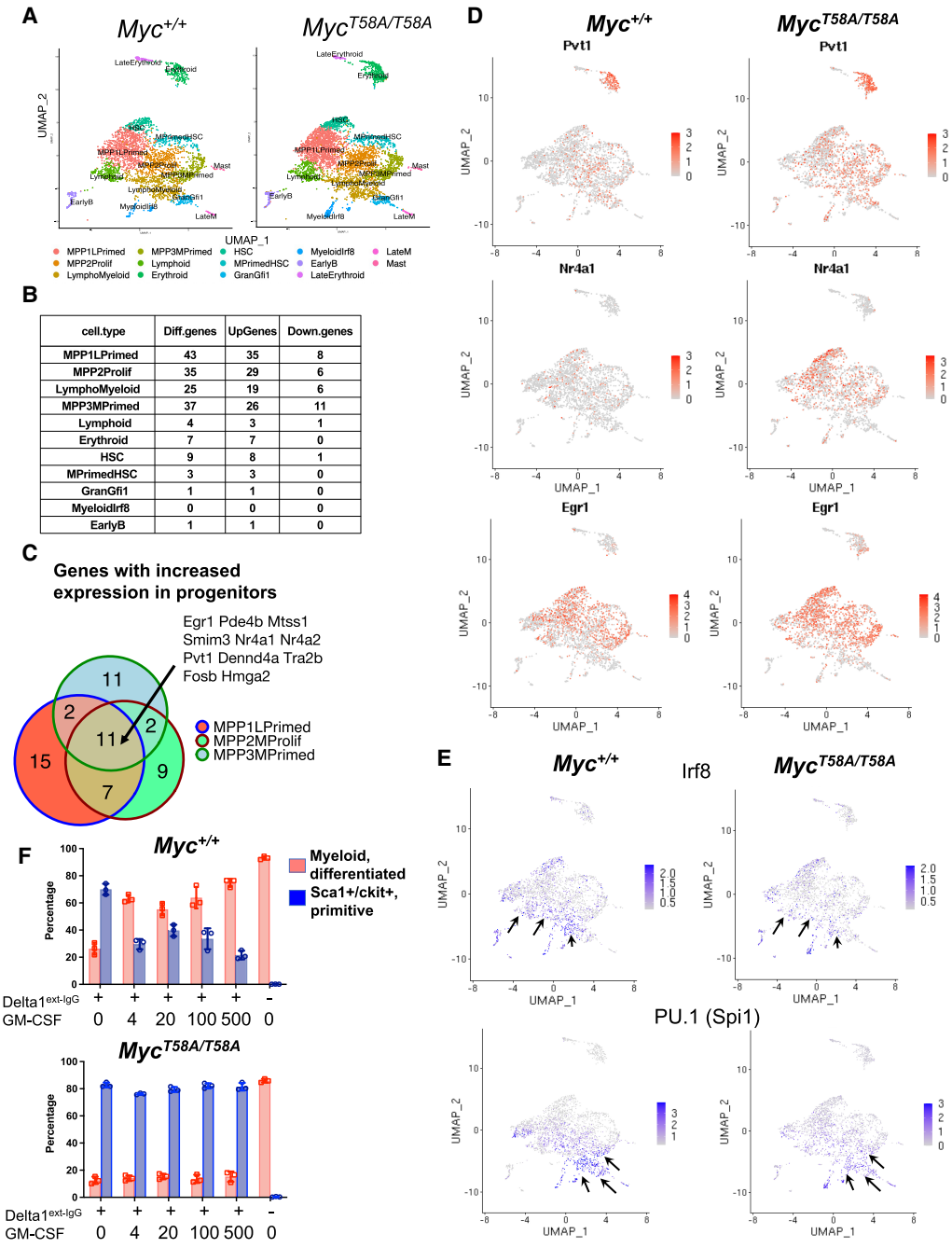

cell.type	Diff.genes	UpGenes	Down.genes
MPP1LPrimed	43	35	8
MPP2Prolif	35	29	6
LymphoMyeloid	25	19	6
MPP3MPrimed	37	26	11
Lymphoid	4	3	1
Erythroid	7	7	0
HSC	9	8	1
MPrimedHSC	3	3	0
GranGfi1	1	1	0
MyeloidIrf8	0	0	0
EarlyB	1	1	0

Figure 3. Single-cell multiome analysis comparing $Myc^{+/+}$ and $Myc^{T58A/T58A}$ hematopoietic stem and progenitor cells. (*A*) Hematopoietic stem and progenitors (LSK-sorted cells) from freshly isolated bone marrow of either $Myc^{+/+}$ or $Myc^{T58A/T58A}$ mutant Myc mice were sorted and barcoded to identify single cells using the 10X Genomics platform for single-cell multiome (RNA-seq and ATAC-seq) analyses. Two mice per genotype were used in two independent experiments to generate four data sets (four mice per genotype, for a total of eight mice). After alignment and analysis using R packages Seurat and Signac (based on RNA content and removal of duplicate barcodes), 7929 cells were included in the analysis. The data sets were then integrated (to account for batch effects) and clustered based on single-cell RNA-seq of $Myc^{+/+}$ and $Myc^{T58A/T58A}$. Following dimension reduction, progenitor cell populations were identified and labeled as detailed in the Materials and Methods. HSCs were set at 0, and cells were ordered along either lymphoid or myeloid pseudotimes. (*B*) The number of differentially expressed (Diff.genes), up-regulated (Up.Genes), and down-regulated (Down.Genes) genes, comparing T58A mutant with WT cells, was determined for each population of progenitor cells. Differentially expressed genes were determined by Wilcoxon rank sum analysis ($P < 0.05$). (*C*) Venn diagram depicting differentially expressed genes in three different hematopoietic progenitor cell populations (MPP1_LPrimed, MPP2_Prolif, and MPP3_MPrimed). Eleven Myc target genes are shown that were up-regulated in $Myc^{T58A/T58A}$ mutant cells in all analyzed progenitor cell populations. (*D*) Heat map of single cells showing the expression of selected genes found to be up-regulated in $Myc^{T58A/T58A}$ mutant progenitor populations. (*E*) Consensus binding motif activity in single-cell ATAC-seq in progenitors in $Myc^{+/+}$ and $Myc^{T58A/T58A}$ mutant mice. (*F*) Hematopoietic progenitor cells were purified from the bone marrow of $Myc^{+/+}$ or $Myc^{T58A/T58A}$ mice (LSK sorting). Sorted cells were then cultured in wells coated with Delta1 ligand to activate the Notch pathway in the presence of cytokine cocktail (see the Materials and Methods). After 2 wk of culture, increasing amounts of GM-CSF were added to the cultures to promote myeloid differentiation. Differentiation was assessed by flow cytometry staining for Sca1/ckit (Sca1/ckit$^+$, primitive), which is retained on primitive cells, and Mac1/Gr1/F480 (myeloid, differentiated) to identify differentiated cells. Asterisks depict significance as assessed by *t*-test. The data shown are representative of two independent experiments with similar results.

consensus binding motif (CACGTG) single-cell score was not increased in MYC-T58A cells relative to wild-type cells (Supplemental Fig. S3G). However, we did note alterations in motifs important in inflammation and differentiation, such as IRF8 and PU.1. These motif scores were diminished in T58A mutant cells, as was evident in relatively differentiated myeloid and lymphoid progenitors (Fig. 3E). This indicates that T58A progenitors may be less poised for both myeloid differentiation and the induction of inflammatory processes during differentiation.

Based on these results, we reasoned that T58A mutant progenitor cells could possess a decreased propensity for differentiating into inflammatory myeloid cells. To test this, LSK-sorted primitive hematopoietic stem and progenitor cells were cultured in Delta ligand to activate the Notch pathway (which promotes primitive lymphopoiesis). These cells were then cultured with increasing amounts of GM-CSF to promote myeloid differentiation. The wild-type cells predominantly differentiated, as >75% of cells began to express myeloid markers, with <20% retaining Sca1 and ckit expression at the highest concentration of GM-CSF (Fig. 3F). Strikingly, only ~15% of T58A cells differentiated into myeloid cells, while >80% retained Sca1/ckit expression even at the highest concentration of GM-CSF (Fig. 3F), although they differentiated normally in the absence of Delta ligand.

Overall, these data characterize a defined set of progenitors in T58A mice that have promiscuous self-renewal capacity prior to malignant progression. Alterations in the self-renewal signature are evident particularly in multipotential progenitors from these mice, consistent with the aberrant self-renewal observed in transplant and replating studies (Fig. 2). Moreover, we found that the T58A progenitors are functionally distinct relative to wild-type progenitors in that, while not present as an overtly expanded population in steady-state hematopoiesis, they nonetheless appear to have a diminished capacity for myeloid differentiation and inflammation when stimulated in culture.

B lymphocytes from $Myc^{T58A/T58A}$ *mice have an altered transcriptome relative to WT lymphocytes*

While a subset of $Myc^{T58A/T58A}$ mice developed myeloid leukemia, a significant number of $Myc^{T58A/T58A}$ mice developed B-cell lymphomas (four out of 12 neoplasms) characterized by B220 and IgM expression (Fig. 1E,F). B-lymphoid progenitor (pre-B) cells from the bone marrow of $Myc^{T58A/T58A}$ mice were resistant to apoptosis and responded differentially to IL7 stimulation (Supplemental Figs. S2H,I, S4A). To better understand the events leading to lymphomagenesis in these mice, we asked what transcriptional alterations are manifested in the B-cell lineage. To this end, we assessed the transcriptional profile of bulk populations of B cells derived from littermate $Myc^{+/+}$ and $Myc^{T58A/T58A}$ mice by comparing B cells derived from the bone marrow and spleen using RNA-seq following mitogen stimulation for 48 h.

In IL7-stimulated pre-B cells, we identified 680 genes with increased expression and 751 genes with decreased expression, comparing T58A with WT controls (FDR < 0.05) (Fig. 4A; Supplemental Fig. S4B). Genes with increased expression in $Myc^{T58A/T58A}$ mice were significantly enriched for known MYC target genes (Fig. 4B). Many of these up-regulated genes were associated with metabolic pathways known to be involved in MYC activation, including glucose metabolism, the mTOR pathway, and nucleotide and fatty acid biosynthesis (Fig. 4B). Importantly, other metabolic pathways activated by MYC in B cells (such as oxidative phosphorylation) were not found to be increased in T58A mutant cells. Hence, cells expressing T58A mutant MYC selectively increased the expression of a subset of MYC target genes.

Differentially expressed genes with relatively decreased expression upon T58A mutation were enriched for inflammatory pathways, especially those associated with interferons and activation by IRF8, NFκB, and Spi1/PU.1 (Fig. 4C; Supplemental Fig. S4C). We also observed down-regulation of MHC class II genes (Supplemental Fig. S4B). Moreover, apoptosis-associated genes were also decreased in T58A mutant pre-B cells (Supplemental Fig. S4C), consistent with our findings that these cells are resistant to apoptosis (Supplemental Fig. S2I,J). In particular, transcription of the proapoptotic effector Bcl2l11 (BIM), a well-established MYC target gene (Muthalagu et al. 2014) that is activated in B cells, was found to be decreased in T58A cells (Supplemental Fig. S4D), in agreement with previous studies of this mutation in the context of MYC overexpression (Hemann et al. 2005).

The RNA-seq results suggested that T58A mutant cells may be more dependent on glucose. In agreement with this, we found that, relative to wild-type cells, T58A mutant pre-B cells exhibited increased uptake of the glucose analog 2-NBDG, indicating a propensity for increased glucose flux, accompanied by an evident decrease in mitochondrial activity (Fig. 4D). Notably, expression of genes encoding rate-limiting enzymes important for glucose metabolism (Ldha and Hk2) were increased in T58A cells (Fig. 4B; Supplemental Fig. S4D). Consistent with these observations, while T58A cells were relatively resistant to the effects of mitochondrial complex I and V inhibitors (metformin and oligomycin, respectively), they were hypersensitive to blockage of glucose uptake (2-deoxyglucose) (Fig. 4E). Together, these data suggest that T58A pre-B cells have an increased rate of glycolysis uncoupled from augmented mitochondrial oxidative phosphorylation, consistent with utilization of the glucose-derived carbon equivalents for increased biosynthesis (nucleotide and fatty acid metabolism). Decreased activation of inflammatory and apoptotic pathways is also consistent with the increased survival and self-renewal of T58A mutant cells.

The transcriptional response of mature B cells to LPS stimulation is profoundly MYC-dependent, as MYC is known to be involved in the amplification of the expression of thousands of genes, many of which are hallmarks of MYC-expressing cells (Nie et al. 2012; Kieffer-Kwon et al. 2017; Tesi et al. 2019). Because T58A mutant cells survive and proliferate at a higher rate relative to wild-type cells and have increased MYC protein in LPS culture

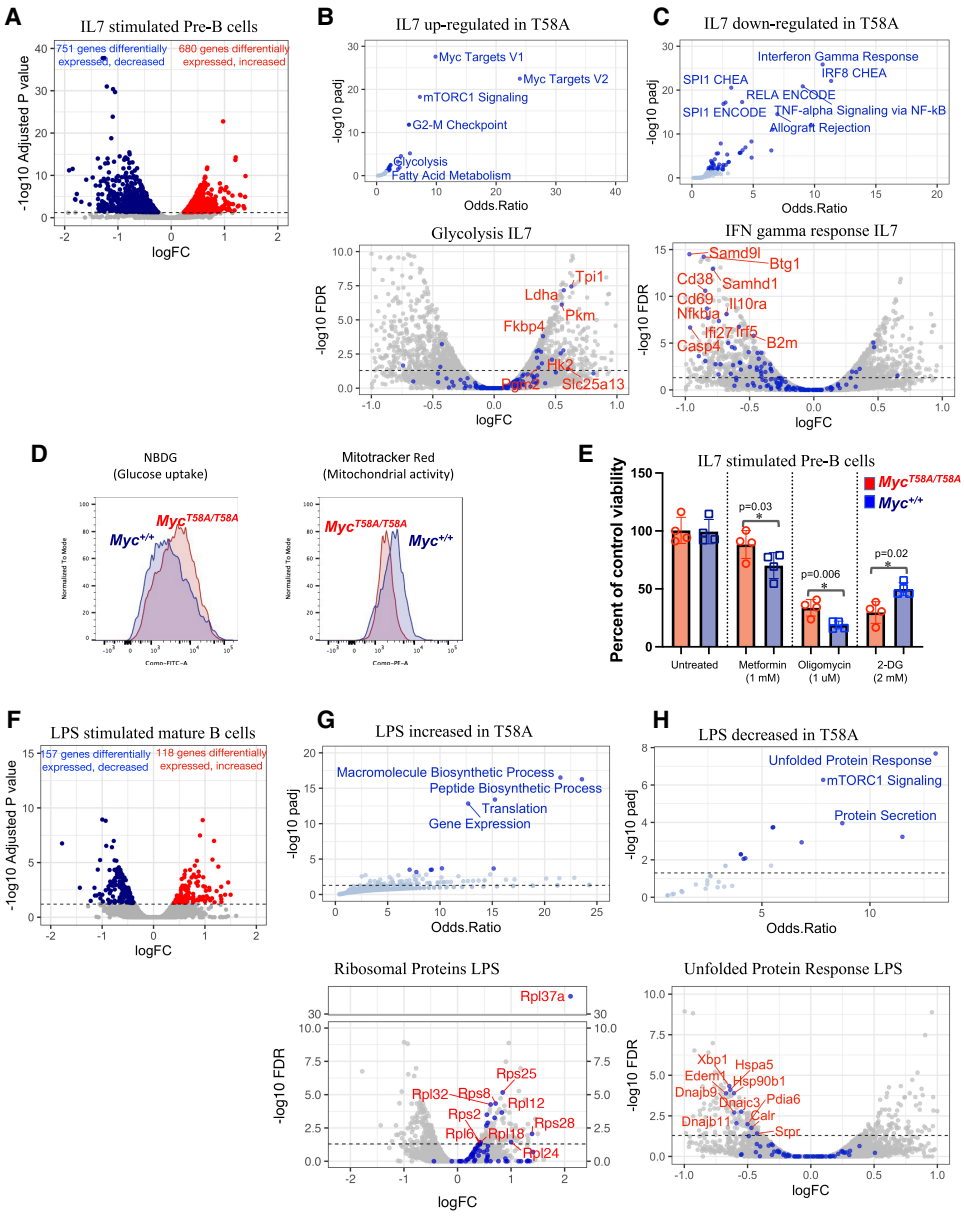

Figure 4. RNA-seq analysis comparing $Myc^{+/+}$ with $Myc^{T58A/T58A}$ mutant pre-B and mature B cells. (*A–C*) IL-7-stimulated B cells derived from bone marrow were sorted from paired littermate WT or T58A mutant mouse bone marrow. RNA was extracted from cells after stimulation with IL-7 for 48 h, and libraries were prepared and barcoded. After sequencing, analysis was performed using EdgeR. (*A*) Differentially expressed genes are depicted in the volcano plot. Genes with decreased expression in $Myc^{T58A/T58A}$ cells are shown in blue, and genes with increased expression are shown in red, with each gene plotted as the $\log_2$ fold change (*x*-axis) against the $-\log_{10}$ transformation of the false discovery rate (FDR; *y*-axis). (*B*,*C*) Enrichment analysis (using EnrichR package) was performed on genes with increased expression in $Myc^{T58A/T58A}$ (*B*) and genes with decreased expression (*C*). (*B*, *top*) A plot depicting enriched pathways from MSigDB hallmark and reactome gene sets. (*Bottom*) A volcano plot showing differentially expressed genes involved in glycolysis (blue symbols) and some genes labeled in red. (*C*, *top*) A plot showing enrichment of down-regulated genes for pathways from MSigDB hallmark and ENCODE/CHEA ChIP-bound transcription factors. (*Bottom*) A volcano plot showing differentially expressed genes involved in interferon response, which are represented by blue symbols. (*D*) Flow cytometry analysis of glucose uptake potential was assessed by incorporation into cells of fluorescent-labeled NBDG (*right* panel) and Mitotracker red (*left* panel) in $Myc^{+/+}$ and $Myc^{T58A/T58A}$ mutant cells stimulated with IL-7. The fluorescent intensity (*x*-axis) is plotted against cell number (*y*-axis). The data shown are representative of three independent experiments with similar results. (*E*) IL-7-stimulated cells were untreated or treated with either mitochondrial inhibitors (metformin or oligomycin) or glucose uptake inhibitor (2-DG) (*x*-axis). Cells were counted and plotted as percent of control untreated cells (*y*-axis). $Myc^{+/+}$ cells are shown in blue, and $Myc^{T58A/T58A}$ cells are shown in red. The results are representative of three independent experiments. (*F–H*) B cells were sorted from $Myc^{+/+}$ or $Myc^{T58A/T58A}$ mutant mouse spleens using anti-B220-coated magnetic beads (MACS). RNA was extracted after stimulation with LPS for 48 h as described above. Paired analysis was performed using the EdgeR package. Genes with decreased expression in $Myc^{T58A/T58A}$ cells are shown in blue, and genes with increased expression are shown in red, with each gene plotted as the $\log_2$ fold change (*x*-axis) against the $-\log_{10}$ transformation of the false discovery rate (FDR; *y*-axis). (*G*,*H*) Enrichment analysis (using EnrichR package) was performed on genes with increased expression in $Myc^{T58A/T58A}$ (*G*) and genes with decreased expression (*H*). (*G*, *top*) A plot depicting enriched pathways (from GO biological process). (*Bottom*) A volcano plot showing differentially expressed genes involved in ribosomal protein biogenesis (blue symbols) and some genes labeled in red. (*H*, *top*) A plot depicting enrichment of genes with decreased expression (MSigDB hallmark gene sets). (*Bottom*) A volcano plot showing differentially expressed genes involved in the unfolded protein response (blue symbols).

(Supplemental Fig. S4E,F), we asked whether we might detect relevant transcriptional changes in this model. We identified a very specific signature from a relatively small number of genes (118 up-regulated genes and 157 down-regulated genes) that were differentially expressed in mature B cells from T58A versus WT mice stimulated with LPS (Fig. 4F; Supplemental Fig. S4G). Genes involved in regulation of protein translation were highly enriched among the set of up-regulated genes, and ribosomal proteins comprised a significantly increased component of this response (Fig. 4G). Strikingly, the major class of down-regulated genes in LPS-stimulated B cells was those involved in the unfolded protein response (UPR) (Fig. 4H). These data further indicate that T58A mutation increases the expression of only a small fraction of MYC-activated genes after LPS stimulation (Supplemental Fig. S4G). Moreover, as the UPR is known to be a MYC-dependent process (Babcock et al. 2013), we surmise that the T58A mutation causes the transcription of these genes to be attenuated compared with WT MYC.

Taken together, the data indicate that T58A mutant MYC alters gene expression of a limited subset of the considerably larger population of MYC target genes in primitive and mature B cells. These changes in gene expression are quite consistent with the increased survival and metabolic rewiring of these cells, and some MYC target gene RNAs were predictably increased. However, many MYC target genes involved in inflammation, apoptosis, and unfolded protein response were decreased in T58A mutant cells.

Analysis of MYC occupancy, RNA polymerase II distribution, and enhancer proximity at differentially expressed genes

Our results show that only a subset of canonical MYC target genes expressed in B lymphocytes is increased or decreased in cells with the T58A mutation, indicating that this mutation primarily affects a subpopulation of genes within the MYC transcriptional program. We anticipated that increased amounts of MYC would occupy promoters of up-regulated genes, since MYC generally activates transcription. To test this, we performed genomic analyses in pre-B cells (stimulated with IL-7) and mature B cells (stimulated using LPS) to identify genomic loci occupied by MYC in WT compared with T58A cells. As expected, we found widespread MYC binding at gene promoters in WT cells, particularly in expressed genes, and in many differentially expressed genes (Fig. 5A,B). Increased occupation of promoters, relative to gene bodies, by T58A mutant MYC was detected in both LPS- and IL-7-stimulated B cells, consistent with increased levels of MYC in these cells (Fig. 5C; Supplemental Fig. S5A,B). However, MYC genomic occupation was generally increased regardless of whether genes exhibited increased, decreased, or unchanged expression levels in MYC-T58A mutant cells. Hence, the gene expression changes are not explained solely by increased amounts of MYC-T58A on promoters. Moreover, clustering of Myc coverage at promoters indicated that the MYC-T58A mutant does not occupy promoters in addition to those bound by wild-type MYC; rather, the increased MYC occupancy occurs at the same loci bound by wild-type MYC (Supplemental Fig. S5A). Since a previous study had shown that promoter affinity for MYC binding is a determinant of promoter occupancy and gene expression (Lorenzin et al. 2016), we assessed whether promoters of differentially expressed loci differed in affinity for MYC-T58A versus WT MYC binding. While we were not able to detect a change in distribution of binding to canonical compared with noncanonical E-box association (Supplemental Fig. S5C), we were able to quantify peak heights of occupied loci as a measure of relative affinity. These data suggested that the most highly up-regulated genes in MYC-T58A cells are those that have relatively high affinity for MYC binding (Supplemental Fig. S5D). Such putative high-affinity bound loci may be the most affected by the increased levels of MYC protein resulting from T58A stabilization.

Because overexpressed MYC has been shown to promote both transcription initiation and elongation during gene expression, we performed ChIP to measure the distribution of RNA polymerase II (Pol2). Genes exhibiting increased expression in T58A cells contained more overall Pol2 reads at both promoters and gene bodies, consistent with their elevated expression (Supplemental Fig. S5E,F). As MYC transcriptional function has been shown to be associated with control of Pol2 pause/release, we determined the Pol2 traveling ratio by comparing promoter-occupied with gene body-occupied RNA Pol2 (Supplemental Fig. S5E–G). Surprisingly, traveling ratios were not significantly altered in MYC-T58A compared with WT MYC cells, indicating that the MYC-T58A mutation does not overtly affect the ratio of promoter-bound to elongating transcripts. Hence, the increased expression of genes seen for T58A mutant Myc may be explained by modestly increased RNA Pol2 loading on promoters and subsequent Pol2 procession through gene bodies in addition to increased H3K27 acetylation (Supplemental Fig. S5E–I).

We noted that differentially expressed genes were often clustered on the genome (e.g., see Supplemental Fig. S5H), prompting us to consider the possibility that differential gene expression due to T58A might be related to the proximity of the clusters to MYC-bound enhancers. We therefore used CUT&RUN to identify enhancers in our WT and T58A mutant cells. Our criteria for enhancer identification included non-promoter-associated peaks containing both H3K27ac and H3K4me2 histone marks and MYC peaks (Supplemental Fig. S5I,J). Similar to promoters, we found elevated levels of MYC-T58A occupation at enhancers (Fig. 5D), again consistent with increased MYC levels in these cells. Interestingly, gene expression changes (comparing WT and T58A mutant cells) appeared dependent on proximity to MYC-bound enhancers in that genes that reside closer to mapped MYC-bound enhancers were significantly more likely to be differentially expressed than genes close to non-MYC-bound enhancers (cumulative distribution P-value of 5×10^{-6} for MYC-bound vs 0.002 for non-MYC-bound enhancers) (Fig. 5E,F; Supplemental Fig. S5I). Furthermore, this association was evident regardless of whether differentially

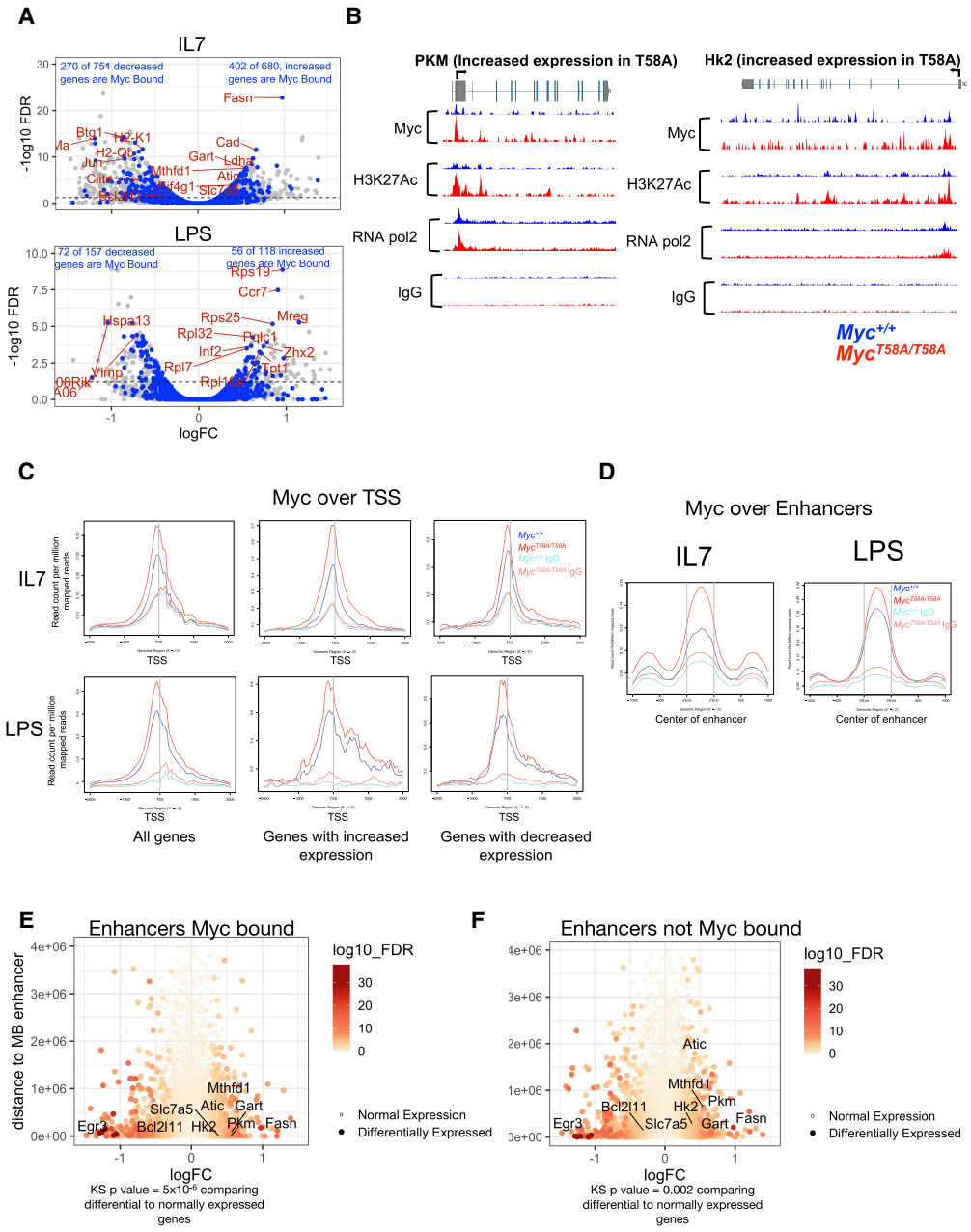

Figure 5. Genomic analysis of Myc at promoters and enhancers in $Myc^{+/+}$ versus $Myc^{T58A/T58A}$ cells. Pre-B or mature B cells sorted from the bone marrow and spleens of $Myc^{+/+}$ and $Myc^{T58A/T58A}$ mice were stimulated with IL-7 (for marrow-derived pre-B cells; *top* panels) and LPS (for mature B cells; *bottom* panels) for 48 h, and 1 million cells were used for auto CUT&RUN to detect Myc, H3K27ac, and H3K3me2, followed by barcoding, sequencing, and alignment. (*A*) MYC-bound genes are shown (dark-blue circles) on the volcano plots depicting the RNA-seq data sets (also shown in Fig. 4) comparing gene expression in $Myc^{T58A/T58A}$ versus $Myc^{+/+}$ B cells stimulated with IL-7 (*left* panel) and LPS (*right* panel). Each gene is plotted as the $\log_2$ fold change (*x*-axis) against the $-\log_{10}$ transformation of the FDR (*y*-axis). Differentially expressed genes are scattered *above* the dotted horizontal line (Padj > 0.05). Genes labeled in red are a sample of differentially expressed genes. The results shown are representative of two biological replicates. (*B*) Genomic tracks showing MYC, H3K27ac, Pol2, and control IgG peaks enriched in CUT&RUN and ChIP-seq (for Pol2) for *Hk2* and *Pkm* genomic loci that have increased expression in $Myc^{T58A/T58A}$ mutant cells. Tracks for $Myc^{+/+}$ cells are shown in blue, and tracks for $Myc^{T58A/T58A}$ cells are shown in red. (*C*) Plots of normalized read counts (*y*-axis) for Myc were generated centered on the TSSs of all genes (*left* panel), genes with increased expression (*middle* panel), and genes with decreased expression (*right* panel). Plots are shown for WT cells (blue) and T58A cells (red). (*D*) Enhancers were identified in WT and T58A mutant IL-7-stimulated pre-B cells (IL-7) and LPS-stimulated mature B cells by peak calls for H3K27ac and H3K4me2 CUT&RUN (see Supplemental Fig. S5F). Enhancers were defined as sites enriched for both marks (and not promoter-bound). Myc CUT&RUN signal was plotted over all identified enhancer peaks for $Myc^{+/+}$ (blue lines) and $Myc^{T58A/T58A}$ (red lines) cells. (*E*) Enhancers that were Myc-bound were identified by Myc peak calls that overlap enhancers. The distance to the nearest Myc-bound enhancer for every gene was calculated. The $\log_2$ fold change for every gene (determined by RNA-seq comparing T58A with WT in IL-7-stimulated pre-B cells) was then plotted (*x*-axis) against the distance to the nearest Myc-bound enhancer (*y*-axis). Differentially expressed genes are represented by filled circles, and the $-\log_{10}$ of the adjusted FDR determined for each gene by RNA-seq is shown by red color intensity. Statistical analysis was performed using two-sample Kolmogorov–Smirnov statistics (cumulative distribution analysis) comparing the distance to the nearest Myc-bound enhancer of each differentially expressed gene (comparing T58A with WT cells) versus the distance to the nearest enhancer of a same-sized random sample of genes activated in lymphocytes but not differentially expressed (see the Materials and Methods). (*F*) Same as *E* except this distance is plotted for the same number of enhancers in *E* that were not Myc-bound (no peaks for Myc).

expressed genes were occupied by Myc (Supplemental Fig. S5K). We collected all the Myc-bound enhancers that were in close proximity (100 kb) to at least one differentially expressed gene in IL-7-stimulated Myc-T58A cells. We found that 444 Myc-bound enhancers were proximal to differentially expressed genes, of which 50 enhancers were proximal to more than two differentially expressed genes (Supplemental Table S1). Correspondingly, approximately half of the differentially expressed genes were proximal (within 100 kb) to Myc-bound enhancers. Myc-bound enhancers were often found in introns of differentially expressed genes (Supplemental Fig. S5J), such as in the Bim (Bcl2l11) locus. H3K27ac was also increased at MYC-bound enhancers in Myc-T58A mutant cells, consistent with increased active chromatin (Supplemental Fig. S5I,J). We surmise that the increased and potentially prolonged association of MYC-T58A (compared with WT MYC) with both enhancers and enhancer-proximal genes results in altered transcription and increased loading of RNA Pol2 on genes with increased expression.

Discussion

We have generated and characterized mice in which a regulatory lymphoma-associated phosphorylation site in c-MYC was inactivated by mutating its normally expressed genomic alleles. This single-amino-acid mutation, threonine 58 to alanine within the conserved phosphodegron, when introduced into the germline is sufficient to predispose mice to leukemia and lymphoma with a relatively long latency. Interestingly, the effects of the T58A point mutation appear confined to the hematopoietic system, highlighting the importance of T58 phosphorylation in regulating normal hematopoiesis. This is consistent with the essential role of MYC in normal hematopoiesis (Laurenti et al. 2008), as well as the association of MYC box I mutations with B-cell lymphomas and myeloid leukemias (Bhatia et al. 1993, 1994; Ferraro et al. 2021). These mutations are thought to be acquired during tumorigenesis and to contribute to oncogenicity. While germline mutations within any MYC-coding regions are rare, several have been noted, including one within the MYC box I phosphodegron (e.g., see https://pecan.stjude.cloud).

In order to address the early events that initiate the neoplasms eventually detected in these mice, we have focused in this report on the premalignant hematopoietic progenitors and B-cell precursors harboring the T58A mutation. These cells display enhanced self-renewal and resistance to apoptosis associated with transcriptional perturbations of MYC target genes. In standard tumor models (e.g., Eμ-Myc) in which MYC is overexpressed or overtly deregulated in mice, affected tissues undergo an initial phase of hyperplasia and perturbed development prior to tumor onset (Langdon et al. 1986; Harris et al. 1988). This is accompanied by increased levels of apoptosis, increased cell cycling, and changes in metabolism. It is noteworthy that in our MYC-T58A mice we did not detect evidence of hyperplasia, increased cell cycling, or apoptosis in multiple tissues. We surmise that the malignancies eventually emerging in these mice are triggered and sustained by the aberrant self-renewal activity and resistance to apoptosis that we observed in T58A hematopoietic progenitor cells. Indeed, many of the gene expression changes and biological properties of the mutant MYC cells are consistent with the baseline characteristics of neoplastic cells; e.g., stem cell-like self-renewal in transplantation experiments, augmented resistance to apoptosis, increased glycolysis, decreased inflammation signaling, and attenuated differentiation potential. Importantly, changes manifested at the single-cell level in the T58A MPP hematopoietic progenitor population are maintained in the more mature hematopoietic cell populations and thus are consistent with the idea that these properties predispose to later cooperating oncogenic mutations (van Lohuizen et al. 1991), which together contribute to evolution of the multiple neoplasms that eventually arise in the T58A mice (Fig. 6).

We hypothesize that the T58 phosphorylation site on MYC normally acts as a switch to regulate or tune gene expression in response to cytokine stimulation. Activation of the PI3K/Akt pathway by cytokines inhibits GSK3β, the kinase that phosphorylates T58, thereby causing T58 to be less phosphorylated (Varano et al. 2017). The change in metabolic state in T58A mutant cells is similar to that seen in germinal center B cells in mice lacking GSK3β (Jellusova et al. 2017). GSK3β normally restricts glucose metabolism and fatty acid biosynthesis and regulates translation and growth, in part by decreasing the abundance of MYC (Jellusova et al. 2017). In contrast, dephosphorylation of T58 by the Phlpp2 phosphatase stabilizes MYC and has been linked to prostate cancer progression (Nowak et al. 2019). Thus, the Myc phosphorylation switch at T58 integrates cell signaling mediated by GSK3β with the MYC transcriptional program. By abrogating FBW7-mediated MYC degradation, T58A mutation activates this metabolic switch independently of its normal regulation by GSK3β. This makes T58 a regulatory target for proliferating, self-renewing cancer cells as a means of altering their metabolic state in response to increased biosynthetic demand. This shift in the gene expression program results in increased dependency on glucose metabolism and protein synthesis and a decreased stress response, which together promote hematopoietic precursor cell survival and self-renewal (Simsek et al. 2010; Ito and Suda 2014). In mature LPS-stimulated B cells, this appears to change the balance between protein synthesis and degradation. MYC is critical for proliferation and survival of mature B cells (Tesi et al. 2019) and induces both ribosomal proteins and the unfolded protein response (Iritani and Eisenman 1999; Babcock et al. 2013). However, in the context of the T58A mutation, this function is skewed toward modest up-regulation of ribosomal protein production but decreased UPR.

Considerable evidence supports the notion that MYC acts as a global amplifier of gene expression, predominantly by facilitating the formation of preinitiation complexes and their transition to elongation (Lin et al. 2012; Nie et al. 2012, 2020). Higher levels of MYC augment RNA polymerase loading and the duration of transcriptional bursting (de Pretis et al. 2017; Patange et al. 2022). As expected, we found promoter occupation by both WT and

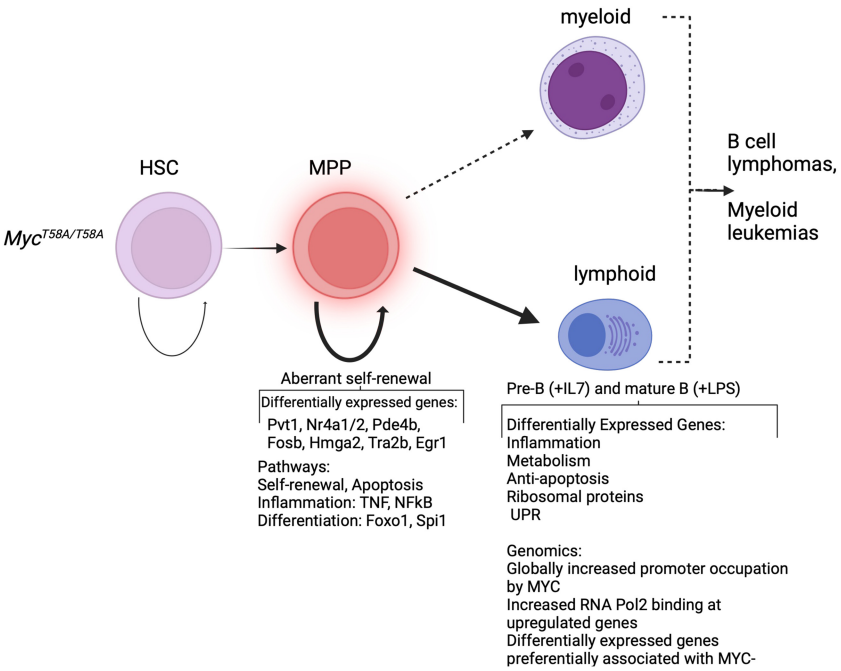

Figure 6. Diagram depicting alterations of hematopoiesis and transcription as a consequence of Myc-T58 phosphorylation. Multipotential progenitors from $Myc^{T58A/T58A}$ mice have an aberrant self-renewal analogous to HSCs and sensitized to leukemias and lymphomas. This is associated with transcriptional changes in genes important in self-renewal of hematopoietic stem and progenitor cells and leukemic cells. Hematopoietic progenitors from $Myc^{T58A/T58A}$ mice are poised away from inflammatory, differentiation, and apoptotic pathways despite increased glycolytic dependence, while genes involved in these processes are proximal to Myc-bound enhancers.

T58A mutant MYC to be widespread. However, T58A promoter occupancy is generally increased (relative to WT MYC) at transcriptional start sites of differentially expressed genes in MYC-T58A cells. This is likely a consequence of the increased abundance of MYC protein due to the T58A block to phosphodegron-mediated turnover. Moreover, our data (based on peak height at MYC-occupied loci) suggest that a subset of up-regulated genes possesses higher apparent affinity for MYC-T58A binding. This is consistent with data using more extensive affinity measurements demonstrating that promoter affinity is a key determinant of MYC-mediated gene regulation (Lorenzin et al. 2016). As expected, we observed an increase in RNA Pol2 occupation at loci with increased expression in MYC-T58A mutant cells.

Importantly, we detected strikingly increased occupancy of enhancers by MYC-T58A relative to WT MYC in both IL-7- and LPS-stimulated B cells. Furthermore, differentially expressed genes were significantly more likely to be located proximal to MYC-bound enhancers, suggesting that the T58A mutant MYC alters promoter–enhancer interactions. It was previously reported that MYC abundance above physiological levels leads to its occupancy of enhancers and promoters through binding to lower-affinity E-boxes (Lorenzin et al. 2016; Zeid et al. 2018). Other studies indicate that MYC controls chromatin structure in B cells to influence transcription and cell state (Kieffer-Kwon et al. 2017; He et al. 2021; See et al. 2022). In the case of MYC-T58A, a more stable form of MYC may exhibit increased dwell time on both enhancers and target promoters, resulting in augmented transcription of enhancer-proximal genes. Conversely, MYC binding may lead to down-regulation of some genes through enhancer interference or a dependence on relatively weaker enhancers (Guo et al. 2018). The switch between phosphorylated and unphosphorylated MYC could therefore act to shift 3D chromatin interactions to alter metabolism and survival. Additional studies focused on higher-order chromatin structure and direct enhancer–promoter interactions will be required to better understand the regulatory landscape imposed by the T58A mutation.

MYC has also been reported to mediate transcriptional repression through both direct and indirect mechanisms (Kaur and Cole 2013; Walz et al. 2014; Patange et al. 2022). However, the loci showing reduced expression in MYC-T58A cells versus WT stimulated B cells (such as proapoptotic Bcl2l11 and UPR stress-associated Xbp1) are normally activated by WT MYC (Muthalagu et al. 2014; de Pretis et al. 2017). Our analysis suggests that these genes are not actively repressed in MYC-T58A cells compared with normal cells but simply are not as strongly activated as in WT cells. Interestingly, we found that many genes exhibiting decreased expression in MYC-T58A mutant cells, relative to WT, are enriched for association with transcription factors regulated by Fbw7 (such as NF-kB/Rel, PU.1, c-JUN, and GFI1), suggesting that the transcriptional effects caused by MYC-T58A mutation may result in a wider perturbation of the Fbw7 degradation network. It is noteworthy that in cells with inactive Fbw7, widespread transcriptional changes correlate with regions of open chromatin (Thirimanne et al. 2022).

MYC is part of an extended network of proteins (e.g., MNT, MGA, and MONDOA) that interact with MAX or the MAX-like protein MLX (for review, see Carroll et al. 2018) and coordinate nutrient availability and cell proliferation. Because MYC-T58A exhibits increased occupancy of promoters and enhancers relative to WT MYC, other network members may potentially compensate by shifting their genomic binding and patterns of gene expression, as has been reported in studies involving perturbation of the network (Cory et al. 2020; Carroll et al. 2021) Furthermore, recent studies implicate additional functions for

MYC involving direct interactions with RNA that may enhance genomic binding and mRNA processing or act to suppress transcriptional stress (Oksuz et al. 2023; Papadopoulos et al. 2023). We anticipate that future studies directed toward both the role of the MYC network and novel activities of MYC will provide insights into precisely how relatively small perturbations in MYC abundance act to initiate neoplasia.

Materials and methods

Generation of T58A mutant mice

To generate a targeting construct replacing the wild-type *Myc* with a *Myc-T58A* mutation, a 2.6-kb fragment (Xba1/HindIII digest) of the *Myc* locus (provided by Andreas Trumpp) harboring the first intron and exon 2 of the coding region was subcloned into pBluescript and mutagenized using Pfu DNA polymerase (Stratagene/Agilent) with primers GAGCTGCTTCCCGCACCGCCCCTGT CCC and GGGACAGGGGCGGTGCGGGAAGCAGC TC. This fragment was inserted downstream from a PGKneo cassette flanked by loxP sites in the pLoxP plasmid (provided by Philippe Soriano). An additional 1.2 kb of sequence (HindIII fragment) containing the 3′ UTR of the *Myc* locus was added at the end (for 3′ homology region). At the 3′ end of the homology region, a diptheria toxin expression cassette was present (PGK-DTA) to facilitate selection of homologous recombination events. An additional 1.4 kb (BglII/Xba1 fragment) was inserted 5′ of the loxP/PGKneo cassette to provide a 5′ homology arm. The resulting targeting construct was then transfected into ES cells (AK-7), selected with G418, and screened by PCR (using primers specific to the targeting construct and flanking DNA), sequencing, and Southern blotting to confirm the mutation and detect proper integration at the *Myc* locus (specify primers and sequence). ES cell clones (two separate clones) exhibiting proper integration were injected into blastocysts and implanted into pseudopregnant female mice to generate chimeric pups. Mice containing the T58A allele were then bred with the MEOX2-CRE transgenic mouse strain, which expresses germline CRE, to excise the intronic PGKneo cassette in the germline (Tallquist and Soriano 2000). Resulting heterozygous mice harboring the mutated T58A allele were bred together in order to produce mice that were homozygous for either the WT or T58A *Myc* alleles ($Myc^{WT/WT}$ or $Myc^{T58A/T58A}$). Two separately identified ES cell clones were identified that transmitted to the germline and gave reproducible results in early experiments. Determination of mouse genotypes was routinely performed using primers that spanned the residual loxP site next to the *c-myc* locus (forward: ACTCGGAGCAGCTGCTAGTC, reverse: TGCACGTCGCTCTGCTGTTG).

Mouse strains and breeding

All mouse experiments were approved and performed at the Fred Hutchinson Cancer Center under International Animal Care and Use Committee protocols (nos. 1195 and 1450). Myc-T58A mice were backcrossed into C57BL/6 mice for all studies. B6.SJL-Ptprc^{a} Pepc^{b}/BoyJ mice (Jackson Laboratories), which express the CD45.1 variant of the *Ptprc* gene, were used as a source of competitor cells and donor mice for competitive repopulation analysis.

Western blotting

Tissues and cell pellets were lysed in RIPA buffer. Lysates were quantified by BCA assay (Pierce) or normalized to cell number for equal loading. Samples were resolved on NuPAGE 4%–12% Bis-Tris gradient gel before being transferred to 0.2-µm nitrocellulose. Blots were blocked with 5% milk in TBST, washed with TBST, and probed with primary antibody to Myc (Cell Signaling Technologies D3N8F) and/or secondary antibody in 5% milk in TBST. The secondary antibody was HRP-conjugated, and chemiluminescent detection was used. Blots were exposed to Pro-Signal blotting film (Genesee Scientific).

Flow cytometry and cell sorting

For RNA-seq, CUT&RUN, and ChIP analysis in B cells, single-cell suspensions of fresh bone marrow or spleen cells were sorted from $Myc^{WT/WT}$ or $Myc^{T58A/T58A}$ mice by positive selection using anti-B220 antibody-conjugated MACS beads for marrow-derived immature B cells or depleted for all other markers in mature B cells from spleens (B-cell isolation kit, Miltenyi Biotech) using an AutoMACS system (Miltenyi Biotech). Analysis of hematopoietic populations from freshly isolated bone marrow, spleen, and thymus cells and sorting of hematopoietic stem cells (HSCs) and progenitor cells (MPPs) was carried out using antibodies (FITC-, APC-, or PE-conjugated) to the following differentiated cell markers: Mac1/CD11b (eBioscience M1/70), Gr1 (eBioscience RB6-8C5), F480 (eBioscience B6), B220 (eBioscience RA3-6B2), CD3e (eBioscience 145-2C11), CD4 (BD Bioscience RM4-5), CD8a (eBioscience 53-6.7), and Ter119 (eBioscience). Analysis and numeration of primitive cells from bone marrow was done using lineage markers with Sca1/Ly6a (PE- or APCcy7-conjugated; eBioscience D7), ckit (PE-, FITC-, or PE-cy7-conjugated; eBioscience 2B8), and CD150 (eBioscience 9D1) antibodies, and proliferating cells were enumerated using Alexa fluor 488-conjugated anti-Ki67 (BD Bioscience B56) antibody. Apoptosis was detected using FITC-labeled VAD–FMK molecules to detect activated caspases (Sigma-Aldrich) or by Annexin V-APC staining (Ebioscience) according to the manufacturer's protocol. B cells were stained for the glucose analog 2-NBDG (Invitrogen) and Mitotracker red (Invitrogen) as directed by the manufacturer. Intracellular staining using antibodies recognizing MYC (Cell Signaling D3N8F), Bim (Cell Signaling C34C5), and Hk2 (Cell Signaling C64G5) was carried out on methanol-fixed cells using intracellular fixation buffer according to the manufacturer (eBiosciences). For sorting HSC and progenitor populations prior to competitive repopulation and single-cell analysis, bone

marrow cells from $Myc^{WT/WT}$ or $Myc^{T58A/T58A}$ mice were first depleted using the purified lineage antibodies described above using either antirat IgG Dynabeads (Thermo Fisher) or MACS lineage depletion beads on an AutoMACS system (Miltenyi Biotech). Cells were then sorted on an Aria3 flow cytometer (Beckton-Dickinson).

Histology and immunohistochemistry

Mice were euthanized at the time of tumor detection, and tissues were collected, fixed in 10% formalin, embedded in paraffin, and stained with hematoxylin and eosin (H&E) using standard methodology. For Ki67 immunohistochemistry, fixed tissues (10% formalin) were submitted to the Fred Hutchinson Cancer Research Center Histology Core for processing. Four-micrometer sections were cut and deparaffinized, followed by heat-induced antigen retrieval. After blocking, Ki67 was detected using a rat anti-Ki67 monoclonal antibody (Dako M7249) at a 1:25 dilution followed by biotinylated goat antirat secondary antibody (Jackson ImmunoResearch 112-065-167) and streptavidin-HRP (Jackson ImmunoResearch 016-030-084). Peripheral blood smears from mice with hematopoietic tumors were stained using Romanowski stain (Diff-quick, Fisher). Pictures were taken using a Nikon E800 microscope.

Competitive repopulation

For competitive repopulation analysis, bone marrow cells were isolated from three WT or Myc-T58A mice, pooled, and sorted for HSCs and MPPs (see "Flow Cytometry and Cell Sorting"). Purified HSCs (four to 100 cells) and MPPs (40–1000 cells) were then mixed with 1×10^6 competitor bone marrow cells isolated from B6.SJL-Ptprc^a Pepc^b/BoyJ mice. Cells were then transplanted via tail vein injection into lethally irradiated (50 cGy) recipient mice (B6.SJL-Ptprc^a Pepc^b/BoyJ). Multilineage hematopoietic reconstitution was then monitored by obtaining peripheral blood every 3 wk from recipient mice followed by staining and flow cytometry analysis for the differentiated cell markers used above (Mac1, Gr1, B220, CD19, CD4, CD8, and F480).

Culture of hematopoietic progenitors and lymphocytes

For culture of hematopoietic progenitor cells in methylcellulose media, unsorted bone marrow cells from $Myc^{+/+}$ or $Myc^{T58A/T58A}$ mice (25,000 cells/mL) were cultured in IMDM containing 50 ng/mL stem cell factor (SCF; Peprotech), 10 ng/mL IL-6 (Peprotech), 10 ng/mL IL-3 (Biovision), 1 ng/mL GM-CSF (Peprotech), 1×10^{-4} M 2-mercaptoethanol, penicillin–streptomycin (10 U/mL penicillin, 10 µg/mL streptomycin), 0.15% methylcellulose (MethoCult, Stem Cell Technologies M3134), and 30% FBS. Hematopoietic progenitor colonies were scored at 7–10 d after culture initiation. For replating experiments, single colonies were picked from the primary cultures, recultured in the same media, and scored 7–10 d later. Sorted hematopoietic stem and progenitor cells from $Myc^{+/+}$ or $Myc^{T58A/T58A}$ (500 LSK sorted cells) were cultured in Delta ligand to activate the Notch pathway. For this, wells of 48-well plates were coated with 5 µg/mL Deltaext-IgG ligand and cultured in IMDM with 100 ng/mL IL-6, SCF, IL-11, and Flt-3 ligand (Biovision). These cultures were maintained by changing media every day. In some experiments, apoptosis was measured by incubating 1 million cells for 1 h in 1 mL/mL FITC–VAD–FMK (EMD-Millipore) to detect apoptotic cells by flow cytometry. For lymphocyte cultures, sorted bone marrow- or spleen-derived B cells were cultured in RPMI with 15% FBS, penicillin–streptomycin, 1×10^{-4} M 2-mercaptoethanol, and either 20 ng/mL IL-7 (Biovision) for bone marrow-derived B cells or 1 µg/mL LPS (Sigma-Aldrich) for mature spleen-derived B cells.

Single-cell analysis

Single-cell analysis was carried out on freshly isolated bone marrow cells from either $Myc^{+/+}$ or $Myc^{T58A/T58A}$ 8-wk-old mice using the 10X Genomics system. Two littermate mice per genotype were sacrificed in two separate experiments (for a total of four mice per genotype) and sorted as described above. Cells were then counted and processed according to the manufacturer's protocol, except that we used a lysis solution with 0.005% digitonin instead of the suggested 0.01% in a 2-min incubation because this produced intact, higher-quality nuclei needed for this experiment. Nuclei were then counted and barcoded, followed by sequencing.

After sequencing, alignment was carried out using Cell Ranger ARC (10X Genomics) for alignment of multiome processed samples. The Cell Ranger ARC output was then read into the R package Seurat (Stuart et al. 2019) and filtered for high-quality single cells with ATAC (RNA amounts between 1000 and 25,000 total reads per cell and <70,000 reads per cell). Data were then processed essentially according to the vignette for integration of independent data sets to identify differentially expressed genes (https://satijalab.org/seurat/articles/integration_introduction). After integration and dimension reduction, categories of stem and progenitor cells were identified. Categorization and labeling of each stem and progenitor category were done by comparison with other recent scRNA-seq data sets (Karamitros et al. 2018; Rodriguez-Fraticelli et al. 2018; Hérault et al. 2021; Konturek-Ciesla et al. 2023), and identifying marks are shown in Supplemental Figure S3A. Most of the more differentiated cell categories were easily defined by expression markers. HSCs were identifiable by expression of primitive markers such as Meis1 (Nestorowa et al. 2016), and a myeloid/megakaryocyte-primed HSC was clearly distinguished by expression of Pbx1 and Vwf (Rodriguez-Fraticelli et al. 2018). Lymphoid progenitors were marked by high levels of Dntt, Flt3, and IL-7R. One population expressed primitive markers with some expression of Flt3 and hence was likely a lymphoid-primed progenitor, which we called MPP1_LPrimed (Belluschi et al. 2018; Konturek-Ciesla et al. 2023). The MPP2 population was mainly characterized by increased expression of proliferation markers (Pol1a and Rad51b) as previously

characterized (Cabezas-Wallscheid et al. 2014), and we called this "MPP2_Prolif." Another progenitor cluster characterized by expression of mitotic markers (Kif20b and Mki67) with relatively high expression of primitive markers was similar to single-cell clusters found previously (Konturek-Ciesla et al. 2023), and we called this population "MPP3_MPrimed." Another population of cells expressed both myeloid (Mpo and Irf8) and lymphoid (Dntt, Flt3, and IL-7R) populations and resembled LMPPs (Karamitros et al. 2018), and we called this LymphoMyeloid.

RNA-seq analysis

Bone marrow-derived pre-B cells or LPS-stimulated mature B cells from littermate pairs of $MYC^{T58A/T58A}$ and control $Myc^{+/+}$ mice were stimulated with 20 ng/mL IL-7 or 1 μg/mL LPS, and RNA was extracted with Trizol reagent and quantified on an Agilent 4200 TapeStation. Five-hundred nanograms of RNA was submitted for library preparation through the Fred Hutchinson Cancer Research Center Genomics Core. After barcoding and sequencing, libraries were aligned to mm10 using TopHat and then processed using the R packages EdgeR and DESeq2 using paired analysis. Further analysis was performed using R scripts for plotting in ggplot2 (volcano plots and heat maps), enrichment analysis using EnrichR, and correlations with other data sets (see "Computational Analysis").

ChIP-seq and CUT&RUN

Genomic binding sites for MYC, H3K27ac, and H3K4me2 were determined using cleavage under targets and release using nuclease (CUT&RUN) automated using the auto CUT&RUN system at the Fred Hutchinson Cancer Research Center (Janssens et al. 2018; Skene et al. 2018). Briefly, primary mouse B cells isolated from bone marrow (for pre-B cells) or spleens (for mature B cells) were prepared fresh or stimulated ex vivo with IL-7 or LPS, respectively. Cells were bound to ConA beads, permeabilized, and incubated overnight with antibody to either c-Myc (Cell Signaling Technologies D3N8F), H3K27ac (Abcam 4729), or H3K4me2 (EMB-Millipore 07030). After digestion with secondary bound protein-A MNase (Henikoff laboratory, Fred Hutchinson Cancer Research Center), the reaction was quenched, and 2 ng of yeast "spike-in" DNA was added. DNA fragments released into the supernatant were collected and directly added without purification into an end repair, and dA tailing reaction was carried out at 58°C (to enhance the capture of small DNA fragments). TruSeq adapters were ligated (rapid DNA ligase; Enzymatics) onto the DNA, and DNA was digested with proteinase K. DNA was then size-fractionated using Ampure beads (Beckman-Coulter), and library preparation was carried out (KAPA Biosystems) by adding barcoded primers. The size distribution was determined for each sample using an Agilent 4200 TapeStation, and the quantity of DNA was determined using Qubit (Invitrogen).

Chromatin immunoprecipitation and sequencing (ChIP-seq) was carried out for RNA Pol2 (which is poorly detected in CUT&RUN) using an MNase digestion step to allow nucleosome resolution of ChIP fragments (Skene and Henikoff 2015). Briefly, after formaldehyde cross-linking, cell lysis, and chromatin fragmentation with MNase, the final SDS concentration after dilution of total chromatin was increased to 0.25% with addition of 20% SDS stock solution. Sonication was performed in a Covaris M220 focused ultrasonicator for 12 min with the following settings: 10% duty cycle, 75-W peak incident power, 200 cycles/burst, and 6°C–7°C bath temperature. The SDS concentration of the sonicated chromatin solution was readjusted to 0.1% with dilution buffer. Immunoprecipitation was performed for RNA Pol2 (Active Motif 4H8) or negative control IgG (Cell Signaling Technology) using 10 μg of antibody for each immunoprecipitation on the clarified chromatin (input) fraction from 10×10^6 cellular equivalents. DNA was then purified using standard phenol:chloroform extraction, and 10 pg of spike-in DNA purified from MNase-digested chromatin from *Saccharomyces cerevisiae* was added to permit comparison between samples. Single-strand library preparation for ChIP samples was then performed as described (Ramani et al. 2019).

Samples were then submitted for 25×25 paired-end sequencing (5 million to 10 million reads for CUT&RUN, and 20 million to 30 million reads for ChIP) on an Illumina HiSeq 2500 instrument at the Fred Hutchinson Cancer Research Center Genomics Shared Resource. Sequences were aligned to the mm10 reference genome assembly using Bowtie2 with the arguments --end-to-end --very-sensitive --no-mixed --no-discordant --overlap --dovetail -I 10 -X 700. Data sets were also aligned to the sc3 (*S. cerevisiae*) assemblies to enumerate reads from spike-in DNA.

Counts per base pair were normalized as previously described by multiplying the fraction of mapped reads spanning each position in the genome by the genome size or by scaling to spike-in DNA. Peak calling was done using the MACS2 package. For H3K27ac and H3K4me2 CUT&RUN data, peaks were called in broad peak mode. Peaks were considered to be associated with a gene if the peak was present within 5 kb of the transcription start site (TSS) or in the gene body. Promoters were defined as the −30:300 base position relative to the TSS.

Computational analysis

Downstream analysis of differentially expressed genes by RNA-seq and correlation with Myc, RNA Pol2 occupation, and chromatin modifications with CUT&RUN, ChIP-seq, and single-cell multiome data was carried out using custom R scripts and functions developed in the Eisenman laboratory. Myc, H3K27ac, and H3K4me2 occupation for enhancer and promoter occupation representing both $Myc^{+/+}$ and $Myc^{T58A/T58A}$ was determined by merging all files together and calling peaks, and this is how enhancers and gene-bound peaks were identified. The GenomicRanges R package was used to process genome positions. Genomic plots were made using ngs.plot (https://github.com/shenlab-sinai/ngsplot) or the R

package ggplot2. Bedtools was also used to numerate genomic positions.

Competing interest statement

R.N.E. is a Scientific Advisory Board Member for Kronos Bio, Inc., and Shenogen Pharma Beijing. There is no overlap with the present study. The other authors declare no competing interests.

Acknowledgments

We are grateful to Pei-Feng Chang for expert assistance in generating the mutant mice, and Michelle Ulrich for maintaining mouse colonies. We thank David Flowers and Cyd McKay for their valuable help with fluorescent cell sorting, Andreas Trumpp and Philippe Soriano for plasmids, and Xiaoying Wu, Yulong Su, and Markus Welcker for critical readings of the manuscript. We also acknowledge the Fred Hutchinson Genomics and Bioinformatics and Comparative Medicine Shared Resources for their excellent technical support. Scientific computing infrastructure was supported by the Office of Research Infrastructure Programs (S10OD028685). This work was supported by National Institutes of Health (NIH) National Cancer Institute grants R35 CA231989 (to R.N.E.) and P01HL084205 (to I.B.), and NIH grant DP2-HG012442 (to V.R.).

Author contributions: B.F. conceived the study, performed the investigaton and formal analysis, and wrote the original draft of the manuscript. P.A.C. performed the investigation and reviewed and edited the manuscript. B.J.V.-F., V.R., and E.L.R. performed the investigation. I.B. conceived the study and acquired funding. R.N.E. conceived and supervised the study, acquired funding, and wrote, reviewed, and edited the manuscript.

References

Adams JM, Harris AW, Pinkert CA, Corcoran LM, Alexander WS, Cory S, Palmiter RD, Brinster RL. 1985. The c-myc oncogene driven by immunoglobulin enhancers induces lymphoid malignancy in transgenic mice. *Nature* **318:** 533–538. doi:10.1038/318533a0

Babcock JT, Nguyen HB, He Y, Hendricks JW, Wek RC, Quilliam LA. 2013. Mammalian target of rapamycin complex 1 (mTORC1) enhances bortezomib-induced death in tuberous sclerosis complex (TSC)-null cells by a c-MYC-dependent induction of the unfolded protein response. *J Biol Chem* **288:** 15687–15698. doi:10.1074/jbc.M112.431056

Belluschi S, Calderbank EF, Ciaurro V, Pijuan-Sala B, Santoro A, Mende N, Diamanti E, Sham KYC, Wang X, Lau WWY, et al. 2018. Myelo–lymphoid lineage restriction occurs in the human haematopoietic stem cell compartment before lymphoid-primed multipotent progenitors. *Nat Commun* **9:** 4100. doi:10.1038/s41467-018-06442-4

Bhatia K, Huppi K, Spangler G, Siwarski D, Iyer R, Magrath I. 1993. Point mutations in the c-Myc transactivation domain are common in Burkitt's lymphoma and mouse plasmacytomas. *Nat Genet* **5:** 56–61. doi:10.1038/ng0993-56

Bhatia K, Spangler G, Gaidano G, Hamdy N, Dalla-Favera R, Magrath I. 1994. Mutations in the coding region of c-myc occur frequently in acquired immunodeficiency syndrome-associated lymphomas. *Blood* **84:** 883–888. doi:10.1182/blood.V84.3.883.883

Butler A, Hoffman P, Smibert P, Papalexi E, Satija R. 2018. Integrating single-cell transcriptomic data across different conditions, technologies, and species. *Nat Biotechnol* **36:** 411–420. doi:10.1038/nbt.4096

Cabezas-Wallscheid N, Klimmeck D, Hansson J, Lipka DB, Reyes A, Wang Q, Weichenhan D, Lier A, von Paleske L, Renders S, et al. 2014. Identification of regulatory networks in HSCs and their immediate progeny via integrated proteome, transcriptome, and DNA methylome analysis. *Cell Stem Cell* **15:** 507–522. doi:10.1016/j.stem.2014.07.005

Carroll PA, Freie BW, Mathsyaraja H, Eisenman RN. 2018. The MYC transcription factor network: balancing metabolism, proliferation and oncogenesis. *Front Med* **12:** 412–425. doi:10.1007/s11684-018-0650-z

Carroll PA, Freie B, Cheng PF, Kasinathan S, Gu H, Hedrich T, Dowdle JA, Venkataramani V, Ramani V, Wu X, et al. 2021. The glucose-sensing transcription factor MLX balances metabolism and stress to suppress apoptosis and maintain spermatogenesis. *PLoS Biol* **19:** e3001085. doi:10.1371/journal.pbio.3001085

Cartwright P, McLean C, Sheppard A, Rivett D, Jones K, Dalton S. 2005. LIF/STAT3 controls ES cell self-renewal and pluripotency by a Myc-dependent mechanism. *Development* **132:** 885–896. doi:10.1242/dev.01670

Chalishazar MD, Wait SJ, Huang F, Ireland AS, Mukhopadhyay A, Lee Y, Schuman SS, Guthrie MR, Berrett KC, Vahrenkamp JM, et al. 2019. MYC-driven small-cell lung cancer is metabolically distinct and vulnerable to arginine depletion. *Clin Cancer Res* **25:** 5107–5121. doi:10.1158/1078-0432.CCR-18-4140

Cho SW, Xu J, Sun R, Mumbach MR, Carter AC, Chen YG, Yost KE, Kim J, He J, Nevins SA, et al. 2018. Promoter of lncRNA gene PVT1 is a tumor-suppressor DNA boundary element. *Cell* **173:** 1398–1412.e22. doi:10.1016/j.cell.2018.03.068

Cory S, Nguyen HV, Vandenberg CJ, Ng AP, Anstee NS, Rimes J, Hawkins E, Robati MR. 2020. Development and survival of MYC-driven lymphomas requires MYC-antagonist MNT to curb MYC-induced apoptosis. *Blood* **135:** 1019–1031. doi:10.1182/blood.2019003014

Dalla-Favera R, Bregni M, Erikson J, Patterson D, Gallo RC, Croce CM. 1982. Human c-myc onc gene is located on the region of chromosome 8 that is translocated in Burkitt lymphoma cells. *Proc Natl Acad Sci* **79:** 7824–7827. doi:10.1073/pnas.79.24.7824

de Pretis S, Kress TR, Morelli MJ, Sabò A, Locarno C, Verrecchia A, Doni M, Campaner S, Amati B, Pelizzola M. 2017. Integrative analysis of RNA polymerase II and transcriptional dynamics upon MYC activation. *Genome Res* **27:** 1658–1664. doi:10.1101/gr.226035.117

Desterke C, Bennaceur-Griscelli A, Turhan AG. 2021. EGR1 dysregulation defines an inflammatory and leukemic program in cell trajectory of human-aged hematopoietic stem cells (HSC). *Stem Cell Res Ther* **12:** 419. doi:10.1186/s13287-021-02498-0

Dhanasekaran R, Deutzmann A, Mahauad-Fernandez WD, Hansen AS, Gouw AM, Felsher DW. 2022. The MYC oncogene—the grand orchestrator of cancer growth and immune evasion. *Nat Rev Clin Oncol* **19:** 23–36. doi:10.1038/s41571-021-00549-2

Eaves CJ. 2015. Hematopoietic stem cells: concepts, definitions, and the new reality. *Blood* **125:** 2605–2613. doi:10.1182/blood-2014-12-570200

Eischen CM, Weber JD, Roussel MF, Sherr CJ, Cleveland JL. 1999. Disruption of the ARF–Mdm2—p53 tumor suppressor pathway in Myc-induced lymphomagenesis. *Genes Dev* **13:** 2658–2669. doi:10.1101/gad.13.20.2658

Farrell AS, Sears RC. 2014. MYC degradation. In *MYC and the pathway to cancer* (ed. Dang CV, Eisenman, RN), pp. 101–115. Cold Spring Harbor Laboraotyr Press, Cold Spring Harbor, NY.

Ferraro F, Miller CA, Christensen KA, Helton NM, O'Laughlin M, Fronick CC, Fulton RS, Kohlschmidt J, Eisfeld AK, Bloomfield CD, et al. 2021. Immunosuppression and outcomes in adult patients with de novo acute myeloid leukemia with normal karyotypes. *Proc Natl Acad Sci* **118:** e2116427118. doi:10.1073/pnas.2116427118

Flinn EM, Busch CM, Wright AP. 1998. Myc boxes, which are conserved in myc family proteins, are signals for protein degradation via the proteasome. *Mol Cell Biol* **18:** 5961–5969. doi:10.1128/MCB.18.10.5961

Gregory MA, Qi Y, Hann SR. 2003. Phosphorylation by glycogen synthase kinase-3 controls c-myc proteolysis and subnuclear localization. *J Biol Chem* **278:** 51606–51612. doi:10.1074/jbc.M310722200

Guo Y, Perez AA, Hazelett DJ, Coetzee GA, Rhie SK, Farnham PJ. 2018. CRISPR-mediated deletion of prostate cancer risk-associated CTCF loop anchors identifies repressive chromatin loops. *Genome Biol* **19:** 160. doi:10.1186/s13059-018-1531-0

Hafemeister C, Satija R. 2019. Normalization and variance stabilization of single-cell RNA-seq data using regularized negative binomial regression. *Genome Biol* **20:** 296. doi:10.1186/s13059-019-1874-1

Harris AW, Pinkert CA, Crawford M, Langdon WY, Brinster RL, Adams JM. 1988. The E mu-myc transgenic mouse. A model for high-incidence spontaneous lymphoma and leukemia of early B cells. *J Exp Med* **167:** 353–371. doi:10.1084/jem.167.2.353

He TC, Sparks AB, Rago C, Hermeking H, Zawel L, da Costa LT, Morin PJ, Vogelstein B, Kinzler KW. 1998. Identification of c-MYC as a target of the APC pathway. *Science* **281:** 1509–1512. doi:10.1126/science.281.5382.1509

He L, Ding Y, Zhao Y, So KK, Peng XL, Li Y, Yuan J, He Z, Chen X, Sun H, et al. 2021. CRISPR/cas9/AAV9-mediated in vivo editing identifies MYC regulation of 3D genome in skeletal muscle stem cell. *Stem Cell Reports* **16:** 2442–2458. doi:10.1016/j.stemcr.2021.08.011

Hemann MT, Bric A, Teruya-Feldstein J, Herbst A, Nilsson JA, Cordon-Cardo C, Cleveland JL, Tansey WP, Lowe SW. 2005. Evasion of the p53 tumour surveillance network by tumour-derived MYC mutants. *Nature* **436:** 807–811. doi:10.1038/nature03845

Hérault L, Poplineau M, Mazuel A, Platet N, Remy E, Duprez E. 2021. Single-cell RNA-seq reveals a concomitant delay in differentiation and cell cycle of aged hematopoietic stem cells. *BMC Biol* **19:** 19. doi:10.1186/s12915-021-00955-z

Iritani BM, Eisenman RN. 1999. c-Myc enhances protein synthesis and cell size during B lymphocyte development. *Proc Natl Acad Sci* **96:** 13180–13185. doi:10.1073/pnas.96.23.13180

Ito K, Suda T. 2014. Metabolic requirements for the maintenance of self-renewing stem cells. *Nat Rev Mol Cell Biol* **15:** 243–256. doi:10.1038/nrm3772

Janssens DH, Wu SJ, Sarthy JF, Meers MP, Myers CH, Olson JM, Ahmad K, Henikoff S. 2018. Automated in situ chromatin profiling efficiently resolves cell types and gene regulatory programs. *Epigenetics Chromatin* **11:** 74. doi:10.1186/s13072-018-0243-8

Jellusova J, Cato MH, Apgar JR, Ramezani-Rad P, Leung CR, Chen C, Richardson AD, Conner EM, Benschop RJ, Woodgett JR, et al. 2017. Gsk3 is a metabolic checkpoint regulator in B cells. *Nat Immunol* **18:** 303–312. doi:10.1038/ni.3664

Karamitros D, Stoilova B, Aboukhalil Z, Hamey F, Reinisch A, Samitsch M, Quek L, Otto GX, Repapi E, Doondeea J, et al. 2018. Single-cell analysis reveals the continuum of human lympho–myeloid progenitor cells. *Nat Immunol* **19:** 85–97. doi:10.1038/s41590-017-0001-2

Kaur M, Cole MD. 2013. MYC acts via the PTEN tumor suppressor to elicit autoregulation and genome-wide gene repression by activation of the Ezh2 methyltransferase. *Cancer Res* **73:** 695–705. doi:10.1158/0008-5472.CAN-12-2522

Kieffer-Kwon KR, Nimura K, Rao SSP, Xu J, Jung S, Pekowska A, Dose M, Stevens E, Mathe E, Dong P, et al. 2017. Myc regulates chromatin decompaction and nuclear architecture during B cell activation. *Mol Cell* **67:** 566–578.e10. doi:10.1016/j.molcel.2017.07.013

Kim SY, Herbst A, Tworkowski KA, Salghetti SE, Tansey WP. 2003. Skp2 regulates Myc protein stability and activity. *Mol Cell* **11:** 1177–1188. doi:10.1016/S1097-2765(03)00173-4

Konturek-Ciesla A, Dhapola P, Zhang Q, Säwén P, Wan H, Karlsson G, Bryder D. 2023. Temporal multimodal single-cell profiling of native hematopoiesis illuminates altered differentiation trajectories with age. *Cell Rep* **42:** 112304. doi:10.1016/j.celrep.2023.112304

Krivtsov AV, Twomey D, Feng Z, Stubbs MC, Wang Y, Faber J, Levine JE, Wang J, Hahn WC, Gilliland DG, et al. 2006. Transformation from committed progenitor to leukaemia stem cell initiated by MLL-AF9. *Nature* **442:** 818–822. doi:10.1038/nature04980

Langdon WY, Harris AW, Cory S, Adams JM. 1986. The c-myc oncogene perturbs B lymphocyte development in Eμ-myc transgenic mice. *Cell* **47:** 11–18. doi:10.1016/0092-8674(86)90361-2

Laurenti E, Varnum-Finney B, Wilson A, Ferrero I, Blanco-Bose WE, Ehninger A, Knoepfler PS, Cheng PF, MacDonald HR, Eisenman RN, et al. 2008. Hematopoietic stem cell function and survival depend on c-Myc and N-Myc activity. *Cell Stem Cell* **3:** 611–624. doi:10.1016/j.stem.2008.09.005

Lin CY, Lovén J, Rahl PB, Paranal RM, Burge CB, Bradner JE, Lee TI, Young RA. 2012. Transcriptional amplification in tumor cells with elevated c-Myc. *Cell* **151:** 56–67. doi:10.1016/j.cell.2012.08.026

Lorenzin F, Benary U, Baluapuri A, Walz S, Jung LA, von Eyss B, Kisker C, Wolf J, Eilers M, Wolf E. 2016. Different promoter affinities account for specificity in MYC-dependent gene regulation. *Elife* **5:** e15161. doi:10.7554/eLife.15161

Mallaney C, Ostrander EL, Celik H, Kramer AC, Martens A, Kothari A, Koh WK, Haussler E, Iwamori N, Gontarz P, et al. 2019. Kdm6b regulates context-dependent hematopoietic stem cell self-renewal and leukemogenesis. *Leukemia* **33:** 2506–2521. doi:10.1038/s41375-019-0462-4

Murphy DJ, Junttila MR, Pouyet L, Karnezis A, Shchors K, Bui DA, Brown-Swigart L, Johnson L, Evan GI. 2008. Distinct thresholds govern Myc's biological output in vivo. *Cancer Cell* **14:** 447–457. doi:10.1016/j.ccr.2008.10.018

Muthalagu N, Junttila MR, Wiese KE, Wolf E, Morton J, Bauer B, Evan GI, Eilers M, Murphy DJ. 2014. BIM is the primary mediator of MYC-induced apoptosis in multiple solid tissues. *Cell Rep* **8:** 1347–1353. doi:10.1016/j.celrep.2014.07.057

Nestorowa S, Hamey FK, Pijuan Sala B, Diamanti E, Shepherd M, Laurenti E, Wilson NK, Kent DG, Göttgens B. 2016. A single-cell resolution map of mouse hematopoietic stem and

progenitor cell differentiation. *Blood* **128:** e20–e31. doi:10.1182/blood-2016-05-716480

Nie Z, Hu G, Wei G, Cui K, Yamane A, Resch W, Wang R, Green DR, Tessarollo L, Casellas R, et al. 2012. c-Myc is a universal amplifier of expressed genes in lymphocytes and embryonic stem cells. *Cell* **151:** 68–79. doi:10.1016/j.cell.2012.08.033

Nie Z, Guo C, Das SK, Chow CC, Batchelor E, Simons SSJ, Levens D. 2020. Dissecting transcriptional amplification by MYC. *Elife* **9:** e52483. doi:10.7554/eLife.52483

Nowak DG, Katsenelson KC, Watrud KE, Chen M, Mathew G, D'Andrea VD, Lee MF, Swamynathan MM, Casanova-Salas I, Jibilian MC, et al. 2019. The PHLPP2 phosphatase is a druggable driver of prostate cancer progression. *J Cell Biol* **218:** 1943–1957. doi:10.1083/jcb.201902048

Nowell P, Finan J, Dalla-Favera R, Gallo RC, ar-Rushdi A, Romanczuk H, Selden JR, Emanuel BS, Rovera G, Croce CM. 1983. Association of amplified oncogene c-myc with an abnormally banded chromosome 8 in a human leukaemia cell line. *Nature* **306:** 494–497. doi:10.1038/306494a0

Oksuz O, Henninger JE, Warneford-Thomson R, Zheng MM, Erb H, Vancura A, Overholt KJ, Hawken SW, Banani SF, Lauman R, et al. 2023. Transcription factors interact with RNA to regulate genes. *Mol Cell* **83:** 2449–2463.e13. doi:10.1016/j.molcel.2023.06.012

Papadopoulos D, Stefanie Anh H, Daniel F, Leonie U, Katharina S, Ivan M, Timothy JR, Annika B, Omkar Rajendra V, Peter G, et al. 2023. Direct RNA-binding by MYCN mediates feedback from RNA processing to transcription control. bioRxiv doi:10.1101/2023.08.16.553474

Patange S, Ball DA, Wan Y, Karpova TS, Girvan M, Levens D, Larson DR. 2022. MYC amplifies gene expression through global changes in transcription factor dynamics. *Cell Rep* **38:** 110292. doi:10.1016/j.celrep.2021.110292

Pulverer BJ, Fisher C, Vousden K, Littlewood T, Evan G, Woodgett JR. 1994. Site-specific modulation of c-Myc cotransformation by residues phosphorylated in vivo. *Oncogene* **9:** 59–70.

Ramani V, Qiu R, Shendure J. 2019. High sensitivity profiling of chromatin structure by MNase-SSP. *Cell Rep* **26:** 2465–2476.e4. doi:10.1016/j.celrep.2019.02.007

Rodriguez-Fraticelli AE, Wolock SL, Weinreb CS, Panero R, Patel SH, Jankovic M, Sun J, Calogero RA, Klein AM, Camargo FD. 2018. Clonal analysis of lineage fate in native haematopoiesis. *Nature* **553:** 212–216. doi:10.1038/nature25168

Salghetti SE, Kim SY, Tansey WP. 1999. Destruction of myc by ubiquitin-mediated proteolysis: cancer-associated and transforming mutations stabilize myc. *EMBO Journal* **18:** 717–726. doi:10.1093/emboj/18.3.717

Scheicher R, Hoelbl-Kovacic A, Bellutti F, Tigan AS, Prchal-Murphy M, Heller G, Schneckenleithner C, Salazar-Roa M, Zöchbauer-Müller S, Zuber J, et al. 2015. CDK6 as a key regulator of hematopoietic and leukemic stem cell activation. *Blood* **125:** 90–101. doi:10.1182/blood-2014-06-584417

Schep AN, Wu B, Buenrostro JD, Greenleaf WJ. 2017. chromVAR: inferring transcription-factor-associated accessibility from single-cell epigenomic data. *Nat Methods* **14:** 975–978. doi:10.1038/nmeth.4401

Schukur L, Zimmermann T, Niewoehner O, Kerr G, Gleim S, Bauer-Probst B, Knapp B, Galli GG, Liang X, Mendiola A, et al. 2020. Identification of the HECT E3 ligase UBR5 as a regulator of MYC degradation using a CRISPR/Cas9 screen. *Sci Rep* **10:** 20044. doi:10.1038/s41598-020-76960-z

Sears R, Nuckolls F, Haura E, Taya Y, Tamai K, Nevins JR. 2000. Multiple Ras-dependent phosphorylation pathways regulate Myc protein stability. *Genes Dev* **14:** 2501–2514. doi:10.1101/gad.836800

See YX, Chen K, Fullwood MJ. 2022. *MYC* overexpression leads to increased chromatin interactions at super-enhancers and MYC binding sites. *Genome Res* **32:** 629–642. doi:10.1101/gr.276313.121

Sheng Y, Ma R, Yu C, Wu Q, Zhang S, Paulsen K, Zhang J, Ni H, Huang Y, Zheng Y, et al. 2021. Role of c-Myc haploinsufficiency in the maintenance of HSCs in mice. *Blood* **137:** 610–623. doi:10.1182/blood.2019004688

Simsek T, Kocabas F, Zheng J, Deberardinis RJ, Mahmoud AI, Olson EN, Schneider JW, Zhang CC, Sadek HA. 2010. The distinct metabolic profile of hematopoietic stem cells reflects their location in a hypoxic niche. *Cell Stem Cell* **7:** 380–390. doi:10.1016/j.stem.2010.07.011

Skene PJ, Henikoff S. 2015. A simple method for generating high-resolution maps of genome-wide protein binding. *Elife* **4:** e09225. doi:10.7554/eLife.09225

Skene PJ, Henikoff JG, Henikoff S. 2018. Targeted in situ genome-wide profiling with high efficiency for low cell numbers. *Nat Protoc* **13:** 1006–1019. doi:10.1038/nprot.2018.015

Smith DP, Bath ML, Metcalf D, Harris AW, Cory S. 2006. MYC levels govern hematopoietic tumor type and latency in transgenic mice. *Blood* **108:** 653–661. doi:10.1182/blood-2006-01-0172

Stuart T, Butler A, Hoffman P, Hafemeister C, Papalexi E, Mauck WM III, Hao Y, Stoeckius M, Smibert P, Satija R. 2019. Comprehensive integration of single-cell data. *Cell* **177:** 1888–1902.e21. doi:10.1016/j.cell.2019.05.031

Stuart T, Srivastava A, Madad S, Lareau CA, Satija R. 2021. Single-cell chromatin state analysis with signac. *Nat Methods* **18:** 1333–1341. doi:10.1038/s41592-021-01282-5

Swartling FJ, Savov V, Persson AI, Chen J, Hackett CS, Northcott PA, Grimmer MR, Lau J, Chesler L, Perry A, et al. 2012. Distinct neural stem cell populations give rise to disparate brain tumors in response to N-MYC. *Cancer Cell* **21:** 601–613. doi:10.1016/j.ccr.2012.04.012

Tallquist MD, Soriano P. 2000. Epiblast-restricted Cre expression in MORE mice: a tool to distinguish embryonic vs. extra-embryonic gene function. *Genesis* **26:** 113–115. doi:10.1002/(SICI)1526-968X(200002)26:2<113::AID-GENE3>3.0.CO;2-2

Tesi A, de Pretis S, Furlan M, Filipuzzi M, Morelli MJ, Andronache A, Doni M, Verrecchia A, Pelizzola M, Amati B, et al. 2019. An early Myc-dependent transcriptional program orchestrates cell growth during B-cell activation. *EMBO Rep* **20:** e47987. doi:10.15252/embr.201947987

Thirimanne HN, Wu F, Janssens DH, Swanger J, Diab A, Feldman HM, Amezquita RA, Gottardo R, Paddison PJ, Henikoff S, et al. 2022. Global and context-specific transcriptional consequences of oncogenic Fbw7 mutations. *Elife* **11:** e74338. doi:10.7554/eLife.74338

Tseng YY, Moriarity BS, Gong W, Akiyama R, Tiwari A, Kawakami H, Ronning P, Reuland B, Guenther K, Beadnell TC, et al. 2014. PVT1 dependence in cancer with MYC copy-number increase. *Nature* **512:** 82–86. doi:10.1038/nature13311

van Lohuizen M, Verbeek S, Scheijen B, Wientjens E, van der Gulden H, Berns A. 1991. Identification of cooperating oncogenes in Eμ-myc transgenic mice by provirus tagging. *Cell* **65:** 737–752. doi:10.1016/0092-8674(91)90382-9

Varano G, Raffel S, Sormani M, Zanardi F, Lonardi S, Zasada C, Perucho L, Petrocelli V, Haake A, Lee AK, et al. 2017. The B-cell receptor controls fitness of MYC-driven lymphoma cells via GSK3β inhibition. *Nature* **546:** 302–306. doi:10.1038/nature22353

Walz S, Lorenzin F, Morton J, Wiese KE, von Eyss B, Herold S, Rycak L, Dumay-Odelot H, Karim S, Bartkuhn M, et al. 2014. Activation and repression by oncogenic MYC shape tumour-specific gene expression profiles. *Nature* **511:** 483–487. doi:10.1038/nature13473

Wang X, Cunningham M, Zhang X, Tokarz S, Laraway B, Troxell M, Sears RC. 2011. Phosphorylation regulates c-Myc's oncogenic activity in the mammary gland. *Cancer Res* **71:** 925–936. doi:10.1158/0008-5472.CAN-10-1032

Welcker M, Orian A, Jin J, Grim JE, Harper JW, Eisenman RN, Clurman BE. 2004. The Fbw7 tumor suppressor regulates glycogen synthase kinase 3 phosphorylation-dependent c-Myc protein degradation. *Proc Natl Acad Sci* **101:** 9085–9090. doi:10.1073/pnas.0402770101

Welcker M, Wang B, Rusnac DV, Hussaini Y, Swanger J, Zheng N, Clurman BE. 2022. Two diphosphorylated degrons control c-Myc degradation by the Fbw7 tumor suppressor. *Sci Adv* **8:** eabl7872. doi:10.1126/sciadv.abl7872

Yada M, Hatakeyama S, Kamura T, Nishiyama M, Tsunematsu R, Imaki H, Ishida N, Okumura F, Nakayama K, Nakayama KI. 2004. Phosphorylation-dependent degradation of c-Myc is mediated by the F-box protein Fbw7. *EMBO J* **23:** 2116–2125. doi:10.1038/sj.emboj.7600217

Zeid R, Lawlor MA, Poon E, Reyes JM, Fulciniti M, Lopez MA, Scott TG, Nabet B, Erb MA, Winter GE, et al. 2018. Enhancer invasion shapes MYCN-dependent transcriptional amplification in neuroblastoma. *Nat Genet* **50:** 515–523. doi:10.1038/s41588-018-0044-9